

# Probing the Higgs self-coupling through double Higgs production in vector boson scattering at the LHC

ERNESTO ARGANDA<sup>1,2\*</sup>, CLAUDIA GARCIA-GARCIA<sup>2†</sup> and MARIA JOSE HERRERO<sup>2‡</sup>

<sup>1</sup>*IFLP, CONICET - Dpto. de Física, Universidad Nacional de La Plata,  
C.C. 67, 1900 La Plata, Argentina*

<sup>2</sup>*Departamento de Física Teórica and Instituto de Física Teórica, IFT-UAM/CSIC,  
Universidad Autónoma de Madrid, Cantoblanco, 28049 Madrid, Spain*

## Abstract

In this work we explore the sensitivity to the Higgs self-coupling  $\lambda$  in the production of two Higgs bosons via vector boson scattering at the LHC. Although these production channels, concretely  $W^+W^- \rightarrow HH$  and  $ZZ \rightarrow HH$ , have lower rates than gluon-gluon fusion, they benefit from being tree level processes, being independent of top physics and having very distinctive kinematics that allow to obtain very clean experimental signatures. This makes them competitive channels concerning the sensitivity to the Higgs self-coupling. In order to give predictions for the sensitivity to this coupling, we first study the role of  $\lambda$  at the subprocess level, both in and beyond the Standard Model, to move afterwards to the LHC scenario. We characterize the  $pp \rightarrow HHjj$  case first and then provide quantitative results for the values of  $\lambda$  that can be probed at the LHC in vector boson scattering processes after considering the Higgs boson decays. We focus mainly in  $pp \rightarrow b\bar{b}b\bar{b}jj$ , since it has the largest signal rates, and also comment on the potential of other channels, such as  $pp \rightarrow b\bar{b}\gamma\gamma jj$ , as they lead to cleaner, although smaller, signals. Our whole study is performed for a center of mass energy of  $\sqrt{s} = 14$  TeV and for various future expected LHC luminosities.

---

\*[ernesto.arganda@fisica.unlp.edu.ar](mailto:ernesto.arganda@fisica.unlp.edu.ar)

†[claudia.garcia@uam.es](mailto:claudia.garcia@uam.es)

‡[maria.herrero@uam.es](mailto:maria.herrero@uam.es)

# 1 Introduction

The Standard Model (SM) of fundamental interactions was finally completed in 2012 with the observation of the Higgs boson by the ATLAS and CMS experiments [1, 2]. Although it allowed to answer many important and well established questions about elementary particle physics, this discovery also posed a lot of new mysteries concerning the scalar sector of the SM.

One of these mysteries is that of the true value of the Higgs self-coupling  $\lambda$ , involved in trilinear and quartic Higgs self-interactions, and its relation to other parameters of the SM. Particularly, understanding and testing experimentally the relation between  $\lambda$  and the Higgs boson mass,  $m_H$ , will provide an excellent insight into the real nature of the Higgs particle. This relation, given in the SM at the tree level by  $m_H^2 = 2v^2\lambda$ , with  $v = 246$  GeV, arises from the Brout-Englert-Higgs (BEH) mechanism [3–6], so to really test this theoretical framework one needs to measure  $\lambda$  independently of the Higgs mass. Unfortunately, the value of the Higgs self-coupling has not been established yet with precision at colliders, but there is (and will be in the future) a very intense experimental program focused on the realization of this measurement (for a review, see for instance [7–11]).

The Higgs trilinear coupling can be probed in double Higgs production processes at the LHC, process that have been extensively studied both theoretically in [11–28], and experimentally in [29–35]. At hadron colliders, these processes can take place through a variety of production channels, being gluon-gluon fusion (GGF) and vector boson scattering (VBS), also called vector boson fusion (VBF) in the literature, the main ones regarding the sensitivity to the Higgs self-coupling. Focusing on the LHC case, on which we will base our posterior study, the dominant contribution to double Higgs production comes from GGF, which for  $\sqrt{s} = 14$  TeV is about a factor 17 larger than from VBS [18]. Because of this, most of the works present nowadays in the literature focus on this particular  $HH$  production channel, GGF, to study the sensitivity to  $\lambda$ . In fact, all these works and the best present measurement at the LHC have made possible to constraint this parameter in the range  $\lambda \in [-8.2, 13.2] \cdot \lambda_{\text{SM}}$  at the 95% CL [35].

Although GGF benefits from the highest statistics and rates, it suffers the inconveniences of having large uncertainties, being a one loop process initiated by gluons, and being dependent of the top Yukawa coupling. Double Higgs production via VBS [8, 11, 13, 16, 18, 19, 22, 24, 26] is, in contrast, a tree level process not initiated by gluons and it is independent of top physics features, leading therefore to smaller uncertainties. Also, at a fundamental level, it is well known that VBS processes involving longitudinally polarized gauge bosons, like the process  $V_L V_L \rightarrow HH$  that we are interested in, probe genuinely the self interactions of the scalar sector of the SM. This would happen specially at high energies, such as those available at the LHC, since, in this regime, each  $V_L$  behaves as its corresponding would-be-Goldstone boson  $\phi$ . Therefore, testing  $V_L V_L \rightarrow HH$  is closely related to testing  $\phi\phi HH$  interactions. In this way, a new window, qualitatively different than GGF, would be open with VBS to test  $\lambda$ , meaning that being able to measure these processes for the first time will be a formidable test of the SM itself, and it could even lead to the discovery of physics beyond the Standard Model (BSM). Moreover, the VBS production channel is the second largest contribution to Higgs pair production, and the VBS topologies have very characteristic kinematics, which allow to select these processes very efficiently as well as to reject undesired backgrounds. In fact, the selection techniques for VBS configurations at the LHC have experienced a great development in the last years and have improved considerably, especially in the context of electroweak (EW) vector boson scattering  $VV \rightarrow VV$  [11, 36–39]. Thus, in summary, VBS double Higgs production might be very relevant to study the sensitivity to the Higgs self-coupling, despite the fact that it is considerably smaller in size than GGF, since it could lead to a cleaner experimental signal. Besides, it will be a complementary measurement to that of GGF and will, in any case, help to improve the determination of this  $\lambda$  coupling with better precision.



Figure 1: Tree level diagrams that contribute to double Higgs production in vector boson scattering in the Unitary gauge. The cyan circle represents the presence of the Higgs self-coupling in the interaction vertex.

In this work, motivated by the above commented advantages, we analyze in full detail Higgs pair production via VBS at the LHC to probe the Higgs self-coupling. To this end, we first explore and characterize the subprocesses of our interest,  $VV \rightarrow HH$  with  $V = W, Z$ , both for the SM with  $\lambda = \lambda_{SM}$  and for BSM scenarios with  $\lambda = \kappa \lambda_{SM}$ , and consider values of  $\kappa$  between 10 and -10. For this study, we fix  $m_H$  to its experimental value,  $m_H = 125.18 \pm 0.16$  GeV [40], and set the Higgs vacuum expectation value (vev) to  $v = 246$  GeV. In this way, studying the sensitivity to  $\lambda$  in VBS will provide the desired independent test of this coupling.

Once we have deeply studied double Higgs production at the subprocess level, we then explore in this work the LHC scenario. First we analyze the process  $pp \rightarrow HHjj$ , to fully understand the properties of this scattering, and then we study and give quantitative results for the sensitivity to the Higgs self-coupling after the Higgs decays. Our main study is performed in the four bottoms and two jets final state,  $pp \rightarrow b\bar{b}b\bar{b}jj$ , since it benefits from the highest rates. We also make predictions for the interesting  $pp \rightarrow b\bar{b}\gamma\gamma jj$  process which, although with lower rates, leads to cleaner signatures. We would like to point out that all computations and simulations are performed at the parton level with no hadronization or detector response simulation taken into account, since the work is aimed to be a first and simple approximation to the sensitivity to  $\lambda$  in VBS processes at the LHC.

The paper is organized as follows: In Section 2 we study VBS double Higgs production at the subprocess level in and beyond the SM. Afterwards, in Section 3, we move on to the LHC case, exploring first the  $pp \rightarrow HHjj$  scattering in Subsection 3.1 and considering later the Higgs decays, both leading  $H \rightarrow b\bar{b}$  decay and subleading  $H \rightarrow \gamma\gamma$  one. Then, we study both signal and background rates for  $pp \rightarrow b\bar{b}b\bar{b}jj$  in Subsection 3.2 and  $pp \rightarrow b\bar{b}\gamma\gamma jj$  in Subsection 3.3, providing our results for the sensitivity to  $\lambda$  in VBS Higgs pair production at the LHC for a center of mass energy of  $\sqrt{s} = 14$  TeV and for different and future expected luminosities. Section 4 summarizes our main conclusions.

## 2 Double Higgs production in vector boson scattering

As already stated in the paragraphs above, we are interested in exploring the sensitivity to the Higgs self-coupling,  $\lambda$ , through VBS processes, in particular at the LHC. For that purpose, we have to study and characterize first the subprocess that leads to the specific signal we will be dealing with once we perform the full collider analysis. This subprocess will be, in our case, the production of two Higgs bosons in the final state from the scattering of two EW gauge bosons,  $VV \rightarrow HH$ , with  $V = W, Z$ . Within this context, in this section we aim to understand the role of the Higgs trilinear coupling in the SM and beyond, as well as the generic characteristics of the scattering processes  $W^+W^- \rightarrow HH$  and  $ZZ \rightarrow HH$ .

The Higgs self-coupling is only present, at the tree level and in the Unitary gauge, in the

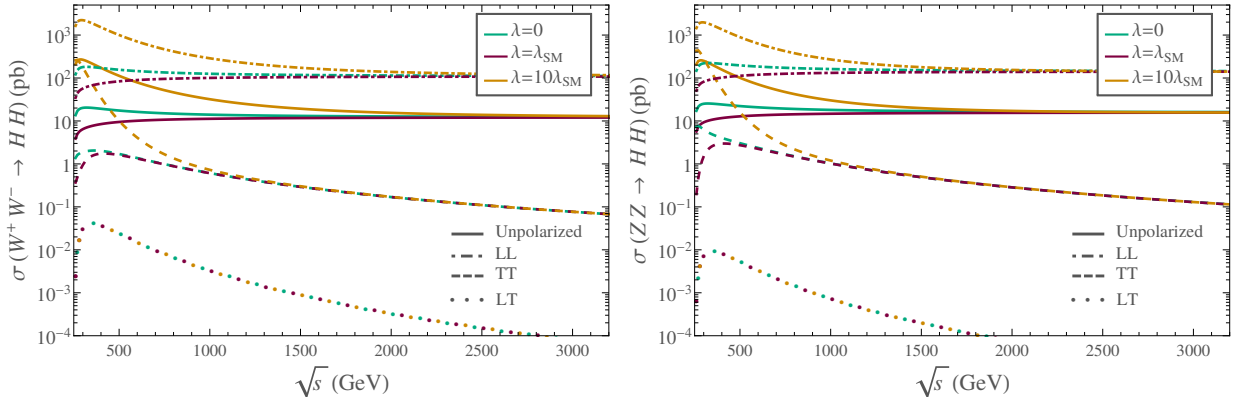


Figure 2: Predictions of the cross sections of  $W^+W^- \rightarrow HH$  (left panel) and  $ZZ \rightarrow HH$  (right panel) as a function of the center of mass energy  $\sqrt{s}$  for three different values of  $\lambda$  and for different polarizations of the initial gauge bosons:  $V_L V_L$  (upper dot-dashed lines),  $V_T V_T$  (middle dashed lines) and  $V_L V_T + V_T V_L$  (lower dotted lines). The unpolarized cross section is also included (solid lines). Each polarized cross section contributes with a factor  $1/9$  to the unpolarized (averaged) cross section.

$s$ -channel diagram of the studied processes, so the sensitivity to  $\lambda$  will only depend on this particular configuration. However, a contact diagram, a  $t$ -channel diagram and a  $u$ -channel diagram have to be taken into account too as shown in Fig. 1, in which we display all the possible tree level contributions to the mentioned scattering processes in the Unitary gauge. Each of these diagrams has its own energy dependence and its own relative size, so they participate differently in the total amplitude  $A(V_1(p_1, \varepsilon_1)V_2(p_2, \varepsilon_2) \rightarrow H_1(k_1)H_2(k_2))$ . This can be seen in Eqs. (1)-(4), where we show the amplitude of each diagram of the process  $W^+W^- \rightarrow HH$ ,  $A_d$ , with  $d = s, c, t, u$  from  $s$ , contact,  $t$  and  $u$  channels respectively, computed consistently in the Unitary gauge:

$$A_s(W^+W^- \rightarrow HH) = 3g^2v^2 \frac{\lambda}{s - m_H^2} (\varepsilon_1 \cdot \varepsilon_2), \quad (1)$$

$$A_c(W^+W^- \rightarrow HH) = \frac{g^2}{2} (\varepsilon_1 \cdot \varepsilon_2), \quad (2)$$

$$A_t(W^+W^- \rightarrow HH) = \frac{g^2}{t - m_W^2} (m_W^2 (\varepsilon_1 \cdot \varepsilon_2) + (\varepsilon_1 \cdot k_1)(\varepsilon_2 \cdot k_2)), \quad (3)$$

$$A_u(W^+W^- \rightarrow HH) = \frac{g^2}{u - m_W^2} (m_W^2 (\varepsilon_1 \cdot \varepsilon_2) + (\varepsilon_1 \cdot k_2)(\varepsilon_2 \cdot k_1)). \quad (4)$$

Here,  $g$  is the EW coupling constant,  $m_W$  is the mass of the  $W$  boson, and  $s, t$  and  $u$  are the usual Mandelstam variables. The amplitudes for the  $ZZ \rightarrow HH$  case are identical except for a global factor  $1/c_w^2$  (with  $c_w = \cos \theta_w$  and with  $\theta_w$  being the weak angle), that has to be included in each amplitude, and the substitution of  $m_W^2$  by  $m_Z^2$  in the  $t$  and  $u$  channel expressions.

On the other hand, the contribution of each polarization state of the initial EW gauge bosons behaves differently, not only energetically, but also in what concerns to the sensitivity to  $\lambda$ . There are only two polarization channels that do depend on  $\lambda$ : the purely longitudinal,  $V_L V_L$ , and the purely transverse in which both vector bosons have the same polarization,  $V_{T+} V_{T+}$  and  $V_{T-} V_{T-}$ . All the other channels have vanishing  $s$ -channel contributions and will not actively participate, therefore, in the study of the Higgs trilinear coupling, although all polarization states contribute to



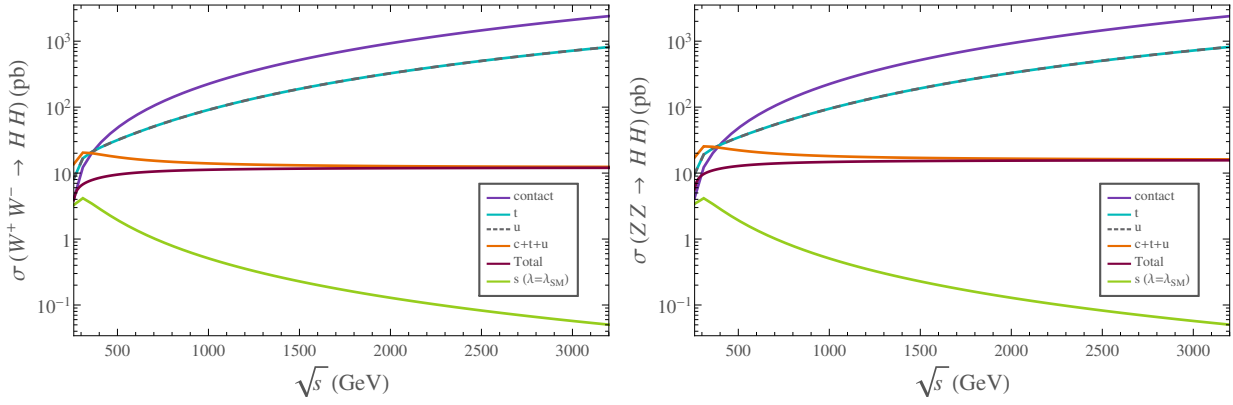


Figure 3: Contribution to the total cross section of  $W^+W^- \rightarrow HH$  (left panel), and of  $ZZ \rightarrow HH$  (right panel) in the SM, i.e.,  $\lambda = \lambda_{SM}$ , of each diagram displayed in Fig. 1 as a function of the center of mass energy  $\sqrt{s}$ . The sum of the contributions of the contact,  $t$ -channel and  $u$ -channel diagrams as well as the sum of all diagrams that contribute are also presented.

the total cross section. Moreover, this total cross section is dominated, specially at high energies, by the purely longitudinal  $V_L V_L$  configuration, and so is each diagram contribution. All these features can be seen in Fig. 2, where we display the predictions for the cross sections of  $W^+W^- \rightarrow HH$  and  $ZZ \rightarrow HH$  as a function of the center of mass energy for three different values of  $\lambda$  separated by polarizations of the gauge bosons, including, also, the unpolarized cross section. In this figure two things are manifest: the first one is that the  $V_L V_T$  configuration is indeed independent of  $\lambda$ . The second one is that the total cross section is clearly strongly dominated by the purely longitudinal contribution at all energies. This is a very interesting result, since it means that, if this process was measured, we would be being sensitive to the purely longitudinal configurations of the gauge bosons, and therefore to the heart of the self-interactions of the SM scalar sector.

The  $V_L V_L$  dominance can be understood through the inspection of the energy dependence of the longitudinal polarization vectors,  $\varepsilon_V$ , at high energies. They are all proportional, for  $\sqrt{s} \gg m_V$ , to a power of the energy over the mass,  $E_V/m_V$ . This leads to a behavior of the amplitudes, presented in Eqs.(2)-(4), for the contact,  $t$  and  $u$  channels respectively, proportional to  $s$ , and to a constant behavior with energy of the  $s$ -channel amplitud given in Eq.(1). Including the extra  $1/s$  suppression factor to compute the cross section from the squared amplitude one obtains the energy dependence seen in Fig. 3, where we present the contribution of each diagram to the total cross sections of  $W^+W^- \rightarrow HH$  and  $ZZ \rightarrow HH$  in the SM, as well as the sum of the contact,  $t$ -channel and  $u$ -channel diagrams,  $(c + t + u)$ , and the total cross section taking all diagrams into account. In this figure, we see clearly that the sum of the contact,  $t$  and  $u$  channels tends at high energy to a constant value. This happens because in the SM there is a cancellation of the linear terms in  $s$  among these three channels. In contrast, the  $s$ -channel contribution decreases as  $1/s$  and is subleading numerically in the SM with respect to the other  $(c + t + u)$  contributions. It is only, at lower energies near the production threshold of two Higgs bosons, where the  $s$ -channel contribution is numerically comparable to the other channels and, in fact, a mild cancellation occurs between this  $s$ -channel and the rest  $(c + u + t)$ . Therefore, the  $s$ -channel and in consequence  $\lambda$ , do not effectively participate in the constant behavior at high energies of the total cross section in the SM. At this point, it is worth recalling that these constant behaviors of the cross sections with energy are characteristic of VBS processes at high energies, precisely because of the above commented

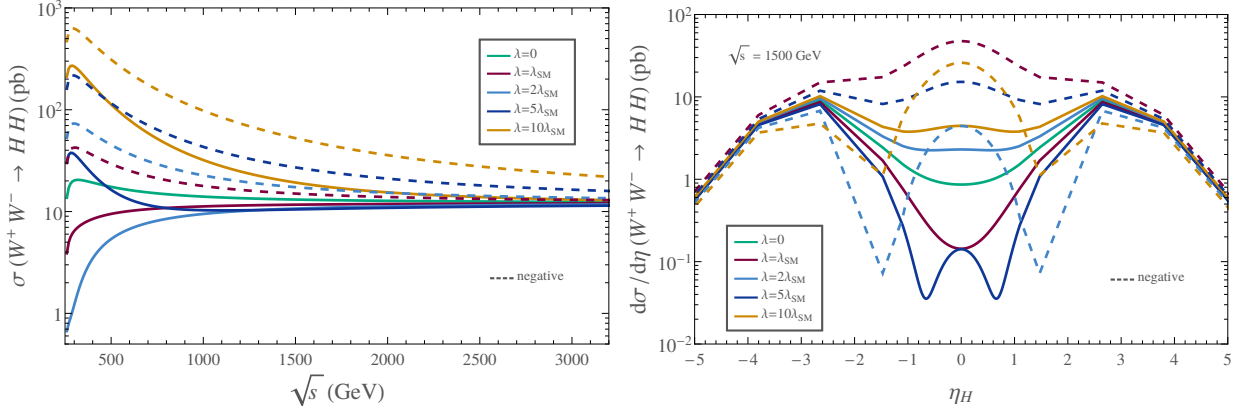


Figure 4: Predictions for the total cross section of the process  $W^+W^- \rightarrow HH$ , as a function of the center of mass energy  $\sqrt{s}$  (left panel) and as a function of the pseudorapidity of one of the final  $H$  at a fixed center of mass energy of  $\sqrt{s} = 1500$  GeV (right panel) for different values of the Higgs self-coupling  $\lambda$ . Solid (dashed) lines correspond to positive (negative) values of  $\lambda$ .

dominance of the longitudinal configurations.

When going beyond the SM by taking  $\lambda \neq \lambda_{SM}$ , the previously described dependence with energy and the delicate cancellations commented above among the various contributing diagrams may change drastically. In fact, varying the size of the Higgs trilinear coupling could modify the relative importance of the contributing diagrams and, in particular, it could allow for the s-channel contribution to be very relevant or even dominate the scattering. This could happen not only at low energies close to the threshold of  $HH$  production, but also at larger energies, where the pattern of cancellations among diagrams could be strongly modified. This may lead to a different high energy behavior, and, hence, to a different experimental signature. The crucial point is that such a large deviation in  $\lambda$  with respect to the SM value is still experimentally possible, as the present bounds on the trilinear coupling are not yet very tight. The best bounds at present set  $\kappa = \lambda/\lambda_{SM} \in [-8.2, 13.2]$  [35], so values of order 10 times the SM coupling are still allowed by LHC data. Then, if in the future the LHC could improve this sensitivity to lower values of  $\lambda$  it would be a formidable test of the presence of new physics beyond the SM. We will show next that this sensitivity can be indeed reached in the future by means of VBS.

It is important to understand in more detail at this point the implications of setting  $\lambda$  to a different value than  $\lambda_{SM}$  in the kinematical properties of the VBS processes we are studying here. For this purpose, we present in Fig. 4 the total cross section of the process  $W^+W^- \rightarrow HH$  as a function of the center of mass energy  $\sqrt{s}$  and the differential cross section with respect to the pseudorapidity  $\eta_H$  of one of the final Higgs bosons (notice that the distribution with respect to the pseudorapidity of the other Higgs particle is the same) for different values of positive, vanishing and negative  $\lambda$ <sup>1</sup>. The results for  $ZZ \rightarrow HH$  (not shown) are very similar to those of  $W^+W^- \rightarrow HH$ . From this figure, it can be seen that, first and most evidently, the total cross section changes in magnitude and in energy dependence with respect to the SM one, as already announced. This happens especially near the  $HH$  production threshold, confirming that the sensitivity to deviations

<sup>1</sup>We assume here a phenomenological approach when setting  $\lambda \neq \lambda_{SM}$ , meaning that it is not our aim to understand the theoretical implications of such a result like potential instabilities for negative values of  $\lambda$ , etc. We understand that the deviations in this coupling would come together with other BSM Lagrangian terms that would make the whole framework consistent.

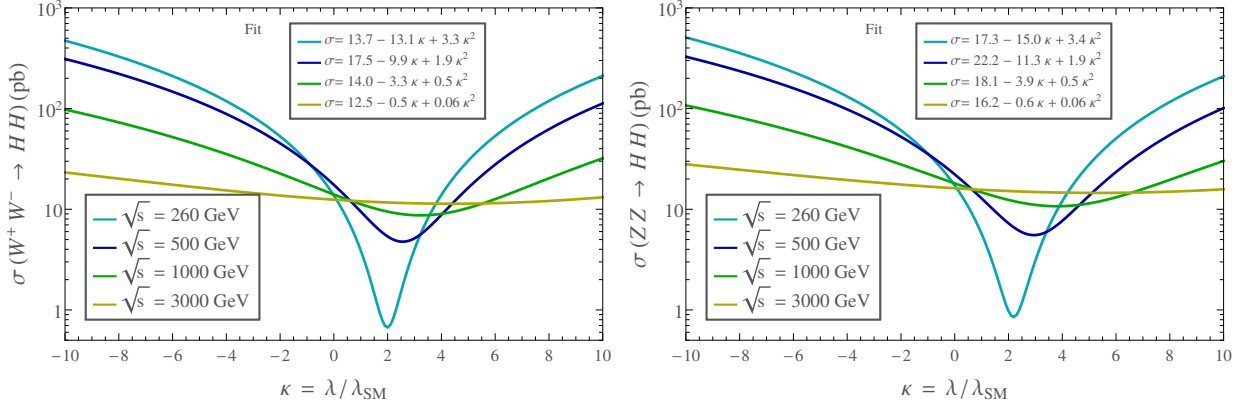


Figure 5: Prediction for the total cross section of the VBS process  $W^+W^- \rightarrow HH$  (left panel) and of  $ZZ \rightarrow HH$  (right panel) as a function of the ratio of a generic  $\lambda$  value over the SM value for four different center of mass energies:  $\sqrt{s} = 260, 500, 1000$  and  $3000$  GeV.

in  $\lambda$  with respect to the SM value is larger in this region. For the case of positive  $\lambda$  the total BMS cross section can be larger or lower than that in the SM, depending on the size of the deviations in  $\lambda$  with respect to  $\lambda_{SM}$ , since in this case there is a destructive interference between the  $s$  channel contribution and the rest ( $c + t + u$ ). In contrast, for the case of negative  $\lambda$  values, the sum of diagrams is always constructive and one obtains bigger cross sections than the SM one independently of the absolute value of the coupling. The details of these features will be extended when commenting the next figure. Regarding the angular dependence of the differential cross section, or correspondingly the distribution respect to  $\eta_H$  also shown in Fig. 4, we see clearly that it also changes in the BSM scenarios respect to the SM one. We particularly learn from this figure that for central values of the Higgs pseudorapidity, concretely for  $|\eta_H| < 2.5$ , it is much easier to distinguish between different values of  $\lambda$ . Therefore, this suggests the kind of optimal cuts in this variable  $\eta_H$ , or the equivalent one in terms of the final particles from the Higgs decays, we should be giving to enhance the sensitivity to the signal when moving to the realistic case of the  $pp$  collisions at the LHC.

In Fig. 5 we display our predictions for the total cross section of the two relevant VBS processes as a function of  $\kappa$  for four different values of fixed center of mass energy  $\sqrt{s} = 260, 500, 1000, 3000$  GeV. We also display the parabolic fits that allow to describe each of the curves to have a more analytical insight into the details of how the above commented cancellations among diagrams do actually occur. The formulas of the fits in this figure manifest that, in general, the cross section has a quadratic, a constant and a linear term in  $\kappa$ , coming, respectively, from the  $s$ -channel contribution, from the  $(c + t + u)$  contribution and from the interference of these two. The sign of the interference is negative for positive values of  $\kappa$  and positive for negative values of  $\kappa$ . This destructive interference for  $\lambda > 0$  produces that the minima of these lines are placed at  $\lambda > \lambda_{SM}$ . Besides, depending on the energy and on the size of  $\kappa$ , the behavior of the cross section will be dominantly constant, linear or quadratic in  $\lambda$ , and therefore the sensitivity to  $\lambda$  will vary accordingly. Near the production threshold, i.e., at energies around 250 GeV, two issues can be seen. The first one is that, as we already saw in Fig. 4, the differences in the cross section when we vary  $\lambda$  are maximal, and so will be the sensitivity to differences in this coupling. The second one is that, at these low energies, the SM, corresponding to  $\kappa = 1$ , suffers, as already said, a mild cancellation between the linear and the constant terms, and therefore the sensitivity to  $\lambda$  will be mainly quadratic. We can also see

that the minima of the parabolas soften, in the sense that the variations in the cross section when we vary  $\lambda$  become smaller, and that their position moves from  $\lambda/\lambda_{SM}$  close to 2 to larger values as the energy is increased. Because of this, the bigger the energy, the bigger the value of  $\lambda$  that maximizes the cancellations. Thus, as a first conclusion at this point, we will have to keep in mind, once we perform the full collider analysis, that the sensitivity to different values of the trilinear coupling and the issue of delicate cancellations among diagrams in VBS are clearly correlated and this will affect the final results at the LHC.

A final comment has to be made in this section, and it is that of a potential unitarity violation problem for large  $|\lambda|$  values in the processes of our interest here,  $VV \rightarrow HH$ . To check this unitarity issue, we have evaluated the partial waves  $a_J$  of the dominant polarization channels for this VBS, which, as we have said, are the longitudinal ones, i.e.,  $V_L V_L \rightarrow HH$ . These  $a_J$  of fixed angular momentum  $J$  are evaluated as usual, by computing:

$$a_J = \frac{1}{64\pi} \int_{-1}^1 d\cos\theta \, A(V_L V_L \rightarrow HH) P_J(\cos\theta), \quad (5)$$

where  $P_J(\cos\theta)$  are the Legendre polynomials. For a given energy,  $\sqrt{s}$ , we then define the unitarity violation limit as the value of  $\lambda$  for which  $|a_J(s)| = 1$ . By doing this exercise, we find that all the partial waves  $|a_J|$  that we have computed are below 0.1 for values of  $\lambda$  between -10 and 10 times the SM value at all energies. So, for the present study, we are safe from unitarity violation problems. For completeness, we have also made a fast estimate of the value of  $\lambda$  that would be required to violate unitarity in this process. For large values of  $|\lambda|$ , the dominant contribution to the total amplitude comes from the  $s$ -channel. This contribution, as we mentioned before, behaves, at high energies and for the purely longitudinal case, as a constant. In particular, one obtains that  $A_s(V_L V_L \rightarrow HH) \sim 6\lambda$  for  $\sqrt{s} \gg m_H$ . With this amplitude, one can compute the value of  $\lambda$  for which the biggest partial wave (in this case we have checked that it is the one corresponding to  $J = 0$ ) becomes one. We obtain  $\lambda_{\text{unit}} \sim 17$ . Notice that this upper limit of  $\lambda$  is above the perturbativity limit given naively by  $\lambda_{\text{pert}} \sim \sqrt{16\pi} \sim 7$ .

With all these features in mind, we can move on from the subprocess level to the full process at the LHC to study the sensitivity of this collider to the Higgs self coupling in VBS processes.

### 3 Sensitivity to the Higgs self-coupling at the LHC

Once we have characterized completely the scattering  $VV \rightarrow HH$ , it is time to explore the full process at the LHC to quantify how sensitive this machine could be to the Higgs trilinear coupling in VBS processes. At this point, we would like to stress again the fact that this double Higgs production channel, via the scattering of two EW gauge bosons, has been poorly studied previously in the literature, due to the fact that it provides less statistics than the GGF one. Nevertheless, now that the LHC is close to reach its nominal energy,  $\sqrt{s} = 14$  TeV, and that it is already achieving high integrated luminosities, close to  $L = 40 \text{ fb}^{-1}$ , the possibility of measuring VBS processes, that were inaccessible before, opens up. In fact, several VBS measurements have been already performed at this collider by ATLAS [41–47] and CMS [48–55]. Taking this into account, and the fact that the kinematics of the VBS processes are incredibly characteristic and allow for a very efficient signal selection and background rejection, a dedicated study of the sensitivity to  $\lambda$  via VBS processes is on demand.

This is precisely the aim of this section, in which we first promote the analysis of Section 2 to that of its LHC signal,  $pp \rightarrow HHjj$ , so that we can fully understand its behavior and properties, and then we give more quantitative and realistic results for the sensitivity to  $\lambda$  once the Higgs

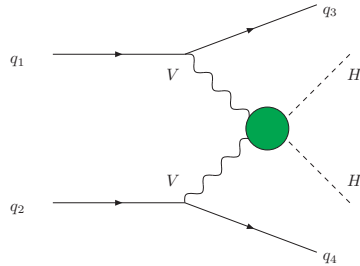


Figure 6: Schematic representation of partonic double Higgs production through VBS at the LHC. The green blob represents the presence of the Higgs self-coupling  $\lambda$  in the process, although all diagrams in Fig.(1) are considered.

bosons have decayed. Specifically, we will focus first on the dominant Higgs decays to bottoms, leading to the process  $pp \rightarrow b\bar{b}b\bar{b}jj$ . This process benefits from having more statistics due to the large branching ratios involved, and, because of this, it is presumably the one that will lead to the best sensitivities. We will also present results on other channels, concretely for  $pp \rightarrow b\bar{b}\gamma\gamma jj$ , where one of the two Higgs bosons has decayed to photons, that, despite their smaller number of events, might also provide interesting results since they suffer from less severe backgrounds.

For all computations and results of the signal events we use MadGraph5@NLO [56], setting the factorization scale to  $Q^2 = m_Z^2$  and using the set of PDF's NNPDF2.3 [57]. We have found that changing the chosen value of  $Q^2$  does not lead to relevant changes in the signal rates. Concerning the backgrounds, all of them are simulated with the same settings and PDF's as the signal, using MadGraph5@NLO as well. For the case of the multijet QCD background in the  $pp \rightarrow b\bar{b}b\bar{b}jj$  channel, due to its complexity, we have simulated events using both MadGraph5 with the previous mentioned settings and PDF's, and AlpGen [58], this time choosing  $Q^2 = (p_{T_b}^2 + p_{T_{\bar{b}}}^2 + \sum p_{T_j}^2)/6$  and selecting the set of PDF's CTEQ5L [59]. We have found agreement between the results of these two MonteCarlos, within the provided errors, in the total normalization of the cross section with the basic cuts, and in the shape of the relevant distributions. All results are presented for a center of mass energy of  $\sqrt{s} = 14$  TeV.

Our study is aimed to be a first and simple approach to the sensitivity to  $\lambda$  in VBS processes at the LHC. This means that, in order to simplify the procedure, the analysis is done at the parton level, and no hadronization or detector response simulation are performed, leaving always room for more expert improvement towards a full and dedicated experimental study.

### 3.1 Study and characterization of $pp \rightarrow HHjj$ signal events

In order to be able to estimate the sensitivity to the Higgs self-coupling in VBS at the LHC, we need to understand how the results of the previous section translate into the full process when we start with protons as initial particles. This full process,  $pp \rightarrow HHjj$ , can be produced via many different channels, and not only in VBS configurations. In fact, it is well known that this VBS subset of diagrams contributing to  $q_1 q_2 \rightarrow q_3 q_4 HH$  is not gauge invariant by itself and all kinds of contributing diagrams have to be included to get gauge invariant result. This is indeed what we are doing here, since when we use MadGraph to compute the signal all kind of diagrams are included.

The crucial point regarding the phenomenological interest of VBS, that indeed motivates this work, is that the specific VBS configuration can be very efficiently selected by choosing the appropriate kinematic regions of the two extra jets variables, as it is well known [28, 36, 37, 39]. In

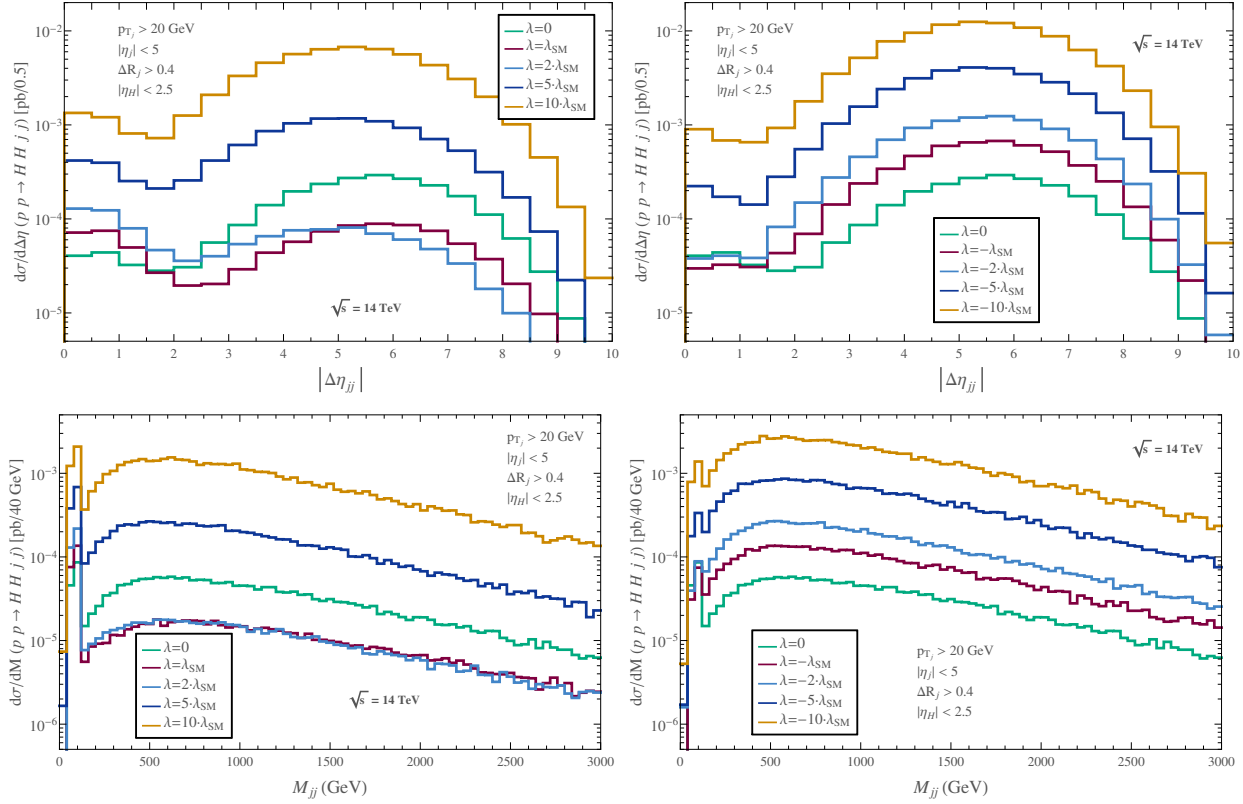


Figure 7: Predictions for the total cross section of the process  $pp \rightarrow HHjj$  as a function of the absolute value of the difference between pseudorapidities of the two jets  $|\Delta\eta_{jj}|$  (upper panels) and as a function of the invariant mass of the two jets  $M_{jj}$  (lower panels) for different values of the Higgs self-coupling  $\lambda$ . We display positive (left panels) and negative (right panels) values of  $\lambda$  for comparison. We also include the case  $\lambda = 0$ . Cuts in Eq.(6) have been applied and the center of mass energy has been set to  $\sqrt{s} = 14$  TeV.

particular, at the LHC, the VBS topologies are characterized by large separations in pseudorapidity of the jets,  $|\Delta\eta_{jj}| = |\eta_{j1} - \eta_{j2}|$ , and by large invariant masses of the dijet system,  $M_{jj}$ . Imposing proper cuts over these two variables makes possible to obtain events that come dominantly from VBS processes and, as we will see later on, also to reject many background events.

The VBS processes involved in  $pp \rightarrow HHjj$  can be seen schematically in Fig. 6, where the green blob represents all diagrams in Fig. 1, including the presence of the  $s$ -channel with the generic Higgs trilinear coupling  $\lambda$ . This kind of processes will inherit the properties of the sub-scatterings we have studied, but will also have differences with respect to them due to the fact that we now have protons in the initial state. Then, it is important to know at this stage how close to the “pure” VBS configuration our  $pp \rightarrow HHjj$  signal is. To this end, we have generated with MadGraph5  $pp \rightarrow HHjj$  signal events for this process for different values of  $\lambda$  with a set of basic cuts that allow for the detection of the final particles, given by:

$$p_{T_j} > 20 \text{ GeV}, \quad |\eta_j| < 5, \quad \Delta R_{jj} > 0.4, \quad |\eta_H| < 2.5, \quad (6)$$

where  $p_{T_j}$  is the transverse momentum of the jets,  $\eta_{j,H}$  is the pseudorapidity of the jets or of the Higgs bosons, and  $\Delta R_{jj}$  is the angular separation between two jets defined as  $\Delta R_{jj} =$



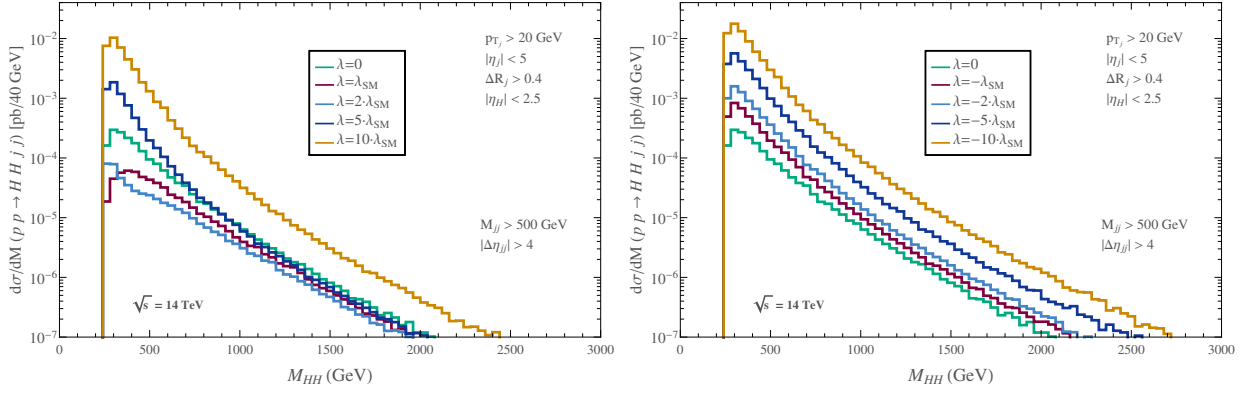


Figure 8: Predictions for the total cross section of the process  $pp \rightarrow HHjj$  as a function of the invariant mass of the di-Higgs system  $M_{HH}$  for different values of the Higgs self-coupling  $\lambda$ . We display positive (left panel) and negative (right panel) values of  $\lambda$  for comparison. We also include the case  $\lambda = 0$ . Cuts in Eq.(6) and VBS selection cuts presented in Eq.(7) have been applied. The center of mass energy has been set to  $\sqrt{s} = 14$  TeV.

$\sqrt{\Delta\eta_{jj}^2 + \Delta\phi_{jj}^2}$ , with  $\Delta\eta_{jj}$  and  $\Delta\phi_{jj}$  being the angular separation in the longitudinal and transverse planes, respectively.

With these generated events, we have studied some relevant distributions for the signal cross section that we have found give the most efficient access to the VBS configuration in  $pp \rightarrow HHjj$  events: distributions with  $M_{jj}$ ,  $\Delta\eta_{jj}$  and  $M_{HH}$ .

In Fig. 7 we present the predictions for the cross section of the process  $pp \rightarrow HHjj$  for different values of  $\lambda$  as a function of the separation in pseudorapidity of the final jets  $|\Delta\eta_{jj}|$  and as a function of the invariant mass of these two jets  $M_{jj}$ . In these plots we can see that our signal is indeed dominated by the VBS configuration, since a very large fraction of the events populate the kinematic regions that correspond to VBS topologies. To have a quantitative estimation, we can take, for instance, the VBS selection cuts proposed in [39] and impose them to the events shown in Fig. 7. Thus, by imposing these cuts:

$$\text{VBS CUTS : } |\Delta\eta_{jj}| > 4, \quad M_{jj} > 500 \text{ GeV}, \quad (7)$$

we obtain that between 50% and 75% (depending on the value of  $\lambda$ , with closer values to 75% for the larger values of  $|\lambda|$ ) of the events are accepted within them, which means that the VBS topologies amount, at least, to half of the total cross section of  $pp \rightarrow HHjj$ . This is indeed a very interesting result, since, as we will see in the forthcoming section, the VBS cuts allow to reduce some backgrounds even in two orders of magnitude. The fact that the signal is practically left unaffected by these cuts is an excellent outcome as the signal to background ratio will favor a better sensitivity to  $\lambda$ .

Furthermore, knowing that the process of our interest at the LHC has a dominant VBS configuration, we would expect the translation from the subprocess results to the complete ones at this level to be straightforward. This appears to be the case, as shown in Fig. 8, where we display the predictions for the total cross section of the process  $pp \rightarrow HHjj$  as a function of the invariant mass of the diHiggs system,  $M_{HH}$ , for different values of the Higgs self-coupling after imposing the cuts given in Eqs. (6) and (7). In these plots, it is manifest that the curves follow the same tendency as the subprocess when we vary  $\lambda$ . Near the  $HH$  production threshold the difference in the cross



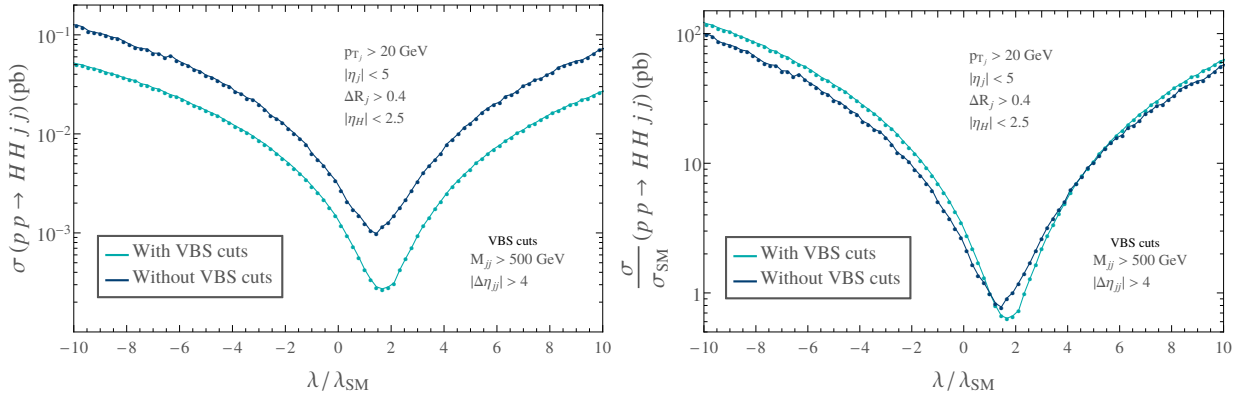


Figure 9: Predictions for the total cross section (left panel) and for the ratio of the total cross section over its SM value (right panel) as a function of the Higgs self-coupling  $\lambda$  with and without imposing the VBS selection cuts given in Eq.(7). Cuts in Eq.(6) have been applied and the center of mass energy has been set to  $\sqrt{s} = 14$  TeV.

sections for different values of the coupling is more pronounced, and one can see again that the cancellations play a role in the same way we learnt at the subprocess level. The SM cross section ( $\kappa = 1$ , in red) lies between the  $\kappa = 0$  (in green) one, which is bigger, and the  $\kappa = 2$  (in light blue) one, which is smaller. Again, for negative values of  $\kappa$  the cross section is always larger than the SM one, so we will have, for the same absolute value of the coupling, better sensitivities for negative  $\lambda$  values.

The issue of the cancellations that take place between the diagram that depends on  $\lambda$  and the rest is shown in more detail in Fig. 9. In this figure, we present the predictions for the total cross section for  $pp \rightarrow HHjj$ , and for the ratio of the total cross section over its SM value as a function of the Higgs self-coupling. We also compare the results with and without imposing the VBS cuts given in Eq.(7) to explore how the cancellation happens at the LHC, and how it depends on the selection of the VBS topologies. We learn again, that, for the same absolute value of  $\lambda$ , negative values give rise to larger cross sections, and therefore to better sensitivities. The smallest cross section corresponds roughly to  $\kappa \sim 1.6$ , which is the value that will be harder to reach at the LHC. One may notice that this value does not coincide exactly with that in Fig. 5, even for the dominant contribution close to the threshold. This slight displacement of the minimum is due to the fact that many different topologies in addition to those of VBS contribute to this final state, in contrast with the results in Fig. 5 that took into account only VBS configurations. In fact, once we apply the VBS cuts the minimum gets closer to that of Fig. 5. Besides, and interestingly, the effect of imposing the VBS selection cuts can ameliorate the sensitivity to  $\lambda$ . Although the cross sections reduce in value after applying the cuts, the ratio of the total cross section for a given trilinear coupling over the SM cross section increases when we are away from the region in which the cancellations are relevant, i.e., for  $\kappa > 3$  and  $\kappa < 1$ .

The last issue we would like to point out in this section refers to the kinematical behavior of the VBS subsystem, that is then translated to the kinematics of the final Higgs bosons. Usually, in vector boson scattering processes at the LHC, most of the energy of the initial  $pp$  state is transmitted to the radiated EW gauge bosons. This leads, as a consequence, to a very boosted system of final  $HH$  pairs, which can be profitable to select these kind of events against backgrounds. If the final Higgs particles are very boosted, their decay products, will have, in general, small angular

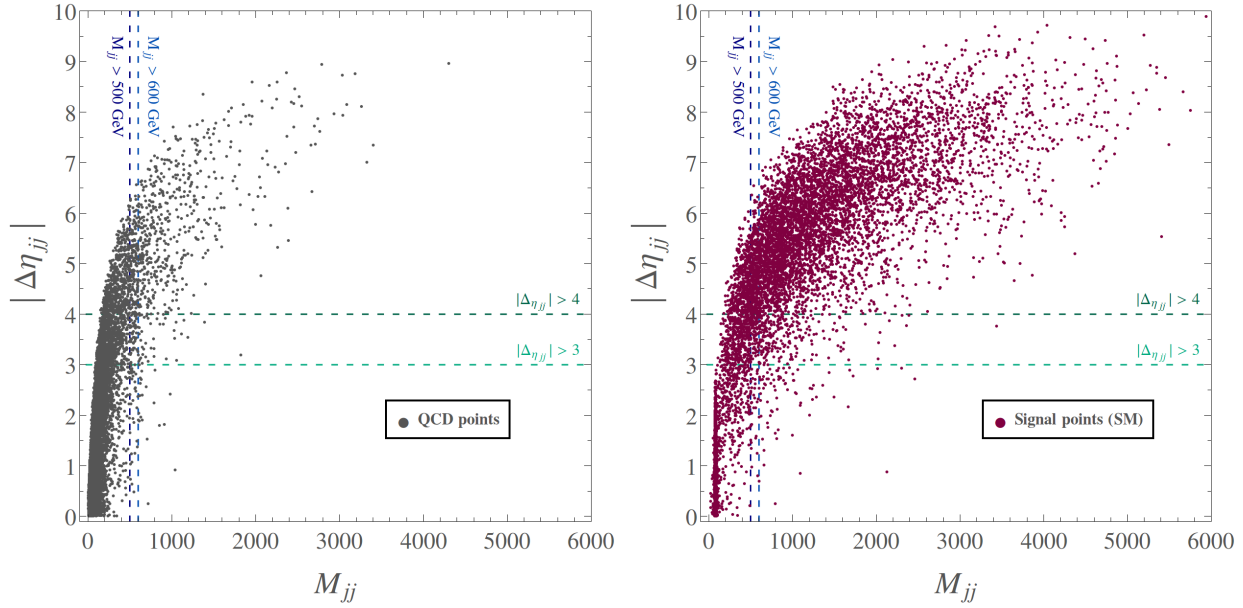


Figure 10: Distribution of 10000 MonteCarlo events of multijet QCD background  $pp \rightarrow b\bar{b}b\bar{b}jj$  (left panel) and signal  $pp \rightarrow HHjj \rightarrow b\bar{b}b\bar{b}jj$  (right panel) in the plane of the absolute value of the difference between pseudorapidities of the two jets  $|\Delta\eta_{jj}|$  versus the invariant mass of the two jets  $M_{jj}$ . Cuts in Eq. (8) have been implemented. The center of mass energy has been set to  $\sqrt{s} = 14$  TeV.

separations. This, together with the fact that the invariant mass of the two particles that come from the Higgs decay has to lie near the Higgs mass, will allow us to characterize very efficiently the Higgs boson candidates as we will see in the next section. With this and the VBS topologies under control, we can study the full processes in which the Higgs bosons have decayed, and compute the sensitivities to  $\lambda$  in these realistic BSM scenarios.

### 3.2 Analysis after Higgs boson decays: sensitivity to $\lambda$ in $pp \rightarrow b\bar{b}b\bar{b}jj$ events

As previously mentioned, once we have fully characterized our most basic process,  $pp \rightarrow HHjj$ , we need to take into account the Higgs decays to perform a realistic analysis at the LHC. The channel we are going to focus on is  $pp \rightarrow b\bar{b}b\bar{b}jj$ , since the decay of the Higgs boson to a bottom-antibottom pair benefits from the biggest branching ratio,  $\text{BR}(H \rightarrow b\bar{b}) \sim 60\%$ . Because of this, we will obtain the largest possible rates for our signal, which will allow us to probe the broadest interval of deviations in the Higgs self-coupling.

Although this process is really interesting because of its large statistics, it is important to mention that it also suffers from having a severe background: the one coming from pure multijet QCD events. This QCD background, of  $\mathcal{O}(\alpha_s^3)$  at the amplitude level, leads to the same final state as our signal,  $pp \rightarrow b\bar{b}b\bar{b}jj$ , and, although in general they have very different kinematics, their rates are so high that some of the events can mimic the signal coming from the decay of two Higgs particles. For this reason, we need to be very efficient when applying selection cuts and criteria to be able to reject this particular background.

We learnt in the previous sections that our signal is very dominated by the VBS configuration. Oppositely, the multijet QCD background is composed primarily by topologies that do not share

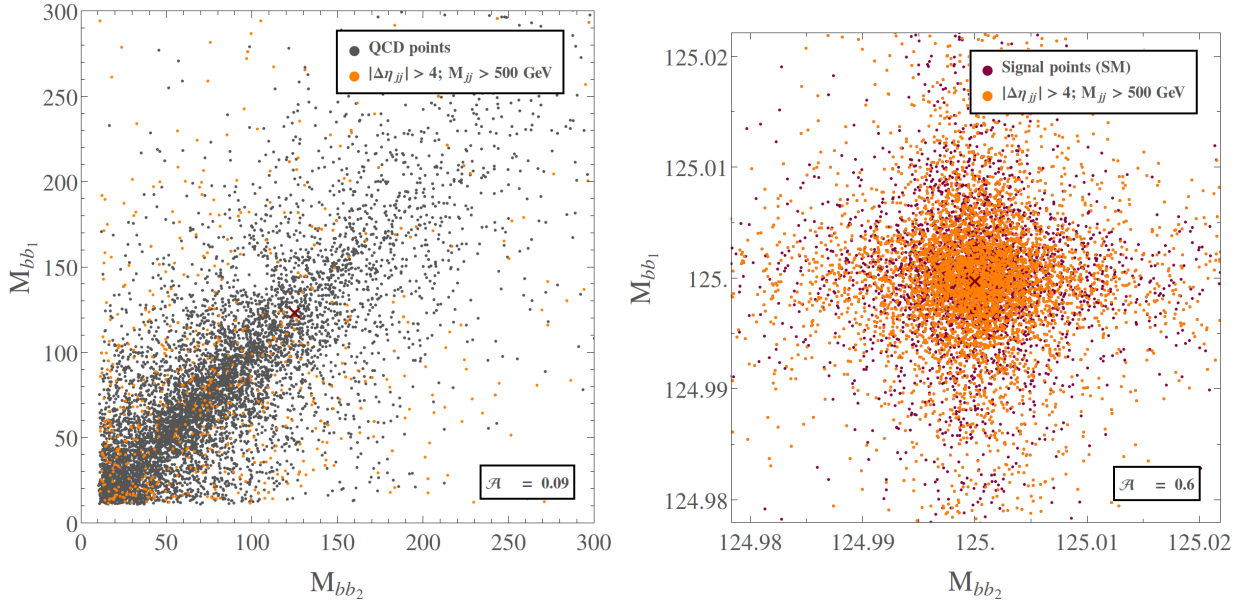


Figure 11: Distribution of 10000 MonteCarlo events of multijet QCD background  $pp \rightarrow b\bar{b}b\bar{b}jj$  (left panel) and signal  $pp \rightarrow HHjj \rightarrow b\bar{b}b\bar{b}jj$  (right panel) in the plane of the invariant mass of one bottom pair identified as a Higgs candidate following the criteria presented in the text  $M_{bb_1}$  versus the invariant mass of the other bottom pair identified as the other Higgs candidate  $M_{bb_2}$ . Black dots correspond to those events that pass the implemented VBS selection cuts given in Eq.(7). Cuts in Eq. (8) have been implemented. The value of the acceptance  $\mathcal{A}$  is also included. The center of mass energy has been set to  $\sqrt{s}=14$  TeV.

kinematical properties with VBS processes. This is the reason why we will first select those QCD events that can be misidentified as those signal events coming from VBS, and take them as a starting point to perform our more refined study of the signal and background.

To have a first insight on how efficient the VBS selection criteria are, we have generated with MadGraph5 ten thousand events for our signal,  $pp \rightarrow HHjj \rightarrow b\bar{b}b\bar{b}jj$  in the SM, i.e.,  $\kappa = 1$ , and for the multijet QCD background with a set of basic cuts that ensure the detection of the final state particles:

$$p_{T_{j,b}} > 20 \text{ GeV}; |\eta_j| < 5; |\eta_b| < 2.5; \Delta R_{jj,jb} > 0.4; \Delta R_{bb} > 0.2. \quad (8)$$

where  $p_{T_{j,b}}$  is the transverse momentum of the jets and bottoms,  $\eta_{j,b}$  are the pseudorapidities of the jets or of the bottom particles, and  $\Delta R_{ij}$  is the angular separation between the  $i$  and  $j$  particles.

In Fig. 10 we display the localization of these events in the  $|\Delta\eta_{jj}| - M_{jj}$  plane, the two variables that better characterize the VBS processes. One can see, indeed, that the QCD events populate mostly the region of small invariant masses of the dijet system and of small differences in pseudo-rapidity of the jets, as opposed, precisely, to the signal events. Thus, imposing the proper VBS cuts, like those in Eq. (7), should relevantly reduce the QCD background leaving the signal nearly unaffected.

In Fig. 11 we aim precisely to see this effect, since we present the same set of events as in Fig. 10 for the QCD background and for the signal highlighting in orange those events that fulfill the VBS selection criteria given in Eq. (7) as an example. This time we show the results in the  $M_{bb_1} - M_{bb_2}$

Set of VBS cuts	$\mathcal{A}_{\text{VBS}}^{\text{QCD}}$	$\mathcal{A}_{\text{VBS}}^{\text{Signal}; \kappa=1}$
$ \Delta\eta_{jj}  > 4, M_{jj} > 500 \text{ GeV}$	0.086	0.631
$ \Delta\eta_{jj}  > 4, M_{jj} > 600 \text{ GeV}$	0.066	0.597
$ \Delta\eta_{jj}  > 4, M_{jj} > 700 \text{ GeV}$	0.054	0.558
$ \Delta\eta_{jj}  > 3, M_{jj} > 500 \text{ GeV}$	0.098	0.669
$ \Delta\eta_{jj}  > 3, M_{jj} > 600 \text{ GeV}$	0.071	0.626
$ \Delta\eta_{jj}  > 3, M_{jj} > 700 \text{ GeV}$	0.057	0.580

Table 1: Predictions for the acceptance of different sets of VBS cuts, including those in Eq. (7), for the multijet QCD background and for the signal with  $\kappa = 1$ . Signal acceptances for the other values of  $\kappa$  considered in the present work,  $\kappa \in [-10, 10]$ , vary between 0.5 and 0.75.

plane, where  $M_{bb_{1,2}}$  are the corresponding invariant masses of the two bottom pairs that are the best candidates to come from the decay of a Higgs boson, as we will see later.

The first thing one can observe in both plots of Fig. 11 is that very few QCD events survive the imposition of the VBS cuts, whereas practically all events of the signal do. The concrete fraction of the events ( $\mathcal{A}$ ) that survive in both cases is also presented in the plots. We call  $\mathcal{A}_{\text{VBS}}$  the acceptance of the VBS cuts, defined as

$$\mathcal{A}_{\text{VBS}} \equiv \frac{\sigma(pp \rightarrow b\bar{b}b\bar{b}jj)|_{\text{VBS}}}{\sigma(pp \rightarrow b\bar{b}b\bar{b}jj)}, \quad (9)$$

i.e., the ratio between the cross section of the process after applying the VBS cuts like those in Eq. (7) over the cross section of the process without having applied them. The basic cuts are imposed in all cases. Taking a look at these numbers, we see that 60% of the signal events pass these cuts while only 9% of the QCD events do. At this point, one might wonder whether these results are very dependent on the specific VBS cuts we impose or not. In Table 1 we show the predictions for the acceptances,  $\mathcal{A}_{\text{VBS}}$ , of different sets of VBS selection cuts, i.e., different cuts in  $|\Delta\eta_{jj}|$  and in  $M_{jj}$ , for both the multijet QCD background and the signal with  $\kappa = 1$ . From those predictions we can see that all the sets of cuts considered lead to very similar results: around 60% of the signal fulfills the VBS selection criteria whereas a 5-10% of the multijet QCD background does. We have checked that for other values of  $\kappa$  the acceptance for the signal varies between a 55% and a 75%. From now on we will apply the VBS selection cuts given in Eq. (7), since this set is well explored in the literature and qualitatively provides the same results as the other sets of cuts that we have analyzed.

The second issue that we can notice about Fig. 11 is that, again, the QCD events populate a very different region of this plane than those of the signal. QCD events tend to lie on low values of  $M_{bb_i}$ , somehow away from the region close to the  $[m_H, m_H]$  point in which most of our signal settles. Evidently, two particles coming from the decay of a Higgs boson should have a total invariant mass value near the Higgs boson mass,  $m_H$ , as our signal does. This motivates the next selection criteria we are going to apply, following the search strategies of ATLAS [32] and CMS [30] for double Higgs production, that are aimed to efficiently identify the  $HH$  candidates.

The  $HH$  candidate identification criteria are also based on what we have learned in the previous sections. Logically, each  $H$  candidate corresponds to a  $b$ -quark pair, and therefore we first need to

define how we are going to pair the final  $b$ -quarks. From now on, it is worth mentioning that we will not distinguish between bottom and anti-bottom, similarly to what is done in experimental analyses. Therefore, with four bottom-like particles in the final state we have three possible double pairings. Among these three possibilities, we select the one in which the values of the invariant masses of the pairs are closer, i.e., the one that minimizes  $|M_{bb_1} - M_{bb_2}|$ , where  $M_{bb_1}$  is the invariant mass of one of the  $bb$  pairs and  $M_{bb_2}$  is the invariant mass of the other pair. Once we have defined the  $b$ -quark pairing, we can profit from the fact that, as mentioned before, if two  $b$ -quarks come from the decay of a boosted Higgs boson, as it happens in VBS processes, the angular separation between them should be small. Thus, we should look for pairs of  $b$ -quarks with small (and yet enough to resolve the particles)  $\Delta R_{bb}$ . Furthermore, we have already discussed that our signal is characterized by the fact that the invariant mass of each  $b$ -quark pair should be around the Higgs mass,  $m_H$ . Therefore, imposing this criterion will ensure that we are maximizing the selection of events that come from the decays of two Higgs bosons.

With all these features in mind, and guided by the ATLAS search strategies [32], we define the following set of cuts as the requirements to efficiently select the candidates to Higgs boson pairs:

*HH* CANDIDATE CUTS :

$$p_{T_b} > 35 \text{ GeV} , \quad (10)$$

$$\hat{\Delta R}_{bb} \equiv \begin{cases} 0.2 < \Delta R_{bb^l} < \frac{653}{M_{4b}} + 0.475; 0.2 < \Delta R_{bb^s} < \frac{875}{M_{4b}} + 0.35, M_{4b} < 1250 \text{ GeV} , \\ 0.2 < \Delta R_{bb^l} < 1; 0.2 < \Delta R_{bb^s} < 1, M_{4b} > 1250 \text{ GeV} , \end{cases} \quad (11)$$

$$\hat{p}_{T_{bb}} \equiv p_{T_{bb^l}} > M_{4b}/2 - 103 \text{ GeV} ; p_{T_{bb^s}} > M_{4b}/3 - 73 \text{ GeV} , \quad (12)$$

$$\chi_{HH} \equiv \sqrt{\left(\frac{M_{bb^l} - m_H}{0.05 m_H}\right)^2 + \left(\frac{M_{bb^s} - m_H}{0.05 m_H}\right)^2} < 1 , \quad (13)$$

where the super-indices  $l$  and  $s$  denote, respectively, leading and subleading, defining the leading  $b$ -quark pair as the one with largest scalar sum of  $p_T$ . One might notice that the requirement of small angular separation between the two  $b$ -quarks of a pair, and the fact that the invariant mass of each  $b$ -quark pair has to lie near the mass of the Higgs, are encoded in the  $\hat{\Delta R}_{bb}$  and in the  $\chi_{HH}$  cuts, respectively. The latter is equivalent to impose that the events in the  $M_{bb_1} - M_{bb_2}$  plane have to lie inside a circle of radius  $0.05 m_H = 6.25 \text{ GeV}$  centered in the point  $[m_H, m_H]$ .

Nevertheless, although multijet QCD events represents the most severe background, there are other processes that can fake our signal. One of them is the  $t\bar{t}$  background, with the subsequent decays of the top quarks and  $W$  bosons,  $t\bar{t} \rightarrow bW^+ \bar{b}W^- \rightarrow b\bar{b}b\bar{b}jj$ . This is, however, a very controlled background, since it is well suppressed by non-diagonal CKM matrix elements and its kinematics are radically different than those of VBS. Starting from a cross section of  $5.4 \cdot 10^{-5} \text{ pb}$  with all the basic cuts in Eq. (8) applied, one ends up in  $1.7 \cdot 10^{-7} \text{ pb}$  after applying the *HH* candidate cuts, and in  $2.0 \cdot 10^{-10} \text{ pb}$  after applying the VBS cuts afterwards. Therefore, since this background is five orders of magnitude smaller than the smallest of our signals, we will neglect it from now onwards.

Finally, we still have to deal with what we call *quasi-irreducible* backgrounds:  $pp \rightarrow HZjj \rightarrow b\bar{b}b\bar{b}jj$  and  $pp \rightarrow ZZjj \rightarrow b\bar{b}b\bar{b}jj$ . These two  $HZ$  and  $ZZ$  production processes, of leading order ( $\alpha \cdot \alpha_S$ ) at the amplitude level, also drive to the same final state as our signal and may give rise to similar kinematics, since they can also take place through VBS configurations. In fact, their rates are very close to those of our signal after applying the VBS selection cuts, that reduce these backgrounds less efficiently than the multijet QCD one. However, we can again take advantage of the fact that the  $b$ -quark pairs have to come from a Higgs boson with a well defined mass. Therefore

Cut	$\sigma_{\text{QCD}}$ [pb]	$\sigma_{ZHjj,ZZjj}$ [pb]	$\sigma_{\text{Signal};\kappa=1}$ [pb]
Basic detection cuts in Eq. (8)	602.72	0.028	$5.1 \cdot 10^{-4}$
$p_{T_b} > 35$ GeV, Eq. (10)	98.31	0.01	$3.0 \cdot 10^{-4}$
$\hat{\Delta}R_{bb}$ , Eq. (11)	33.80	$6.3 \cdot 10^{-3}$	$1.1 \cdot 10^{-4}$
$\hat{p}_{T_{bb}}$ , Eq. (12)	29.77	$5.8 \cdot 10^{-3}$	$9.0 \cdot 10^{-5}$
$\chi_{HH} < 1$ , Eq. (13)	$7.9 \cdot 10^{-2}$	$8.6 \cdot 10^{-6}$	$9.0 \cdot 10^{-5}$
VBS cuts in Eq. (7)	$6.8 \cdot 10^{-3}$	$5.5 \cdot 10^{-6}$	$4.1 \cdot 10^{-5}$

Table 2: Predictions for the total cross section of the multijet QCD background, of the combined  $pp \rightarrow HZjj \rightarrow b\bar{b}b\bar{b}jj$  and  $pp \rightarrow ZZjj \rightarrow b\bar{b}b\bar{b}jj$  background and of the signal with  $\kappa = 1$  after imposing each of the cuts given in Eq. (8) and in Eqs. (10)-(13) subsequently. We show as well the total cross section after applying, afterwards, the VBS selection cuts in Eq. (7).

the  $HH$  candidate cuts should allow us to reject these backgrounds.

In Table 2 we present the cross sections of the multijet QCD background, of the combined  $pp \rightarrow HZjj \rightarrow b\bar{b}b\bar{b}jj$  and  $pp \rightarrow ZZjj \rightarrow b\bar{b}b\bar{b}jj$  background and of the signal with  $\kappa = 1$ , with the basic cuts already set, after applying each of the cuts in Eqs.(10)-(13) subsequently. This way, we see the reduction factor after each cut, and the total cross section of both signal and background once we have performed our complete  $HH$  candidate selection. We show as well the effect of applying the VBS cuts given in Eq. (7) afterwards, since we have checked that both sets of cuts ( $HH$  candidate cuts and VBS cuts) are practically independent. Thus, we have the total cross sections of the two main backgrounds and of our SM signal after applying all the selection criteria. In Table 3 we provide the total cross sections of the signal for all the values of  $\lambda$  considered in this work, again after applying all the selection criteria, for comparison.

From the results in Table 2 we can learn that the sum of the two *quasi-irreducible* backgrounds,  $ZHjj+ZZjj$ , is under control after applying the  $HH$  candidate cuts, since its cross section lies an order of magnitud below the SM signal. On the other hand, the multijet QCD background remains being very relevant even after imposing all the selection criteria. However, as we will see later, the total reduction that it suffers still allows to be sensitive to interesting values of  $\kappa$  even for low luminosities. This reduction, along with that suffered by the *quasi-irreducible* backgrounds and with that suffered by the SM signal, is presented in Table 4. There we show the acceptances of the

$\kappa$	0	1	-1	2	-2	5	-5	10	-10
$\sigma_{\text{Signal}} \cdot 10^4$ [pb]	1.9	0.4	5.0	0.4	9.7	10.1	33.2	56.4	102.6

Table 3: Predictions for the total cross section of the signal  $pp \rightarrow b\bar{b}b\bar{b}jj$  after imposing all the selection criteria, VBS cuts given in in Eq. (7) and  $HH$  candidate cuts given in Eqs. (10)-(13) for all the values of  $\kappa$  considered in this work:  $\kappa = 0, \pm 1, \pm 2, \pm 5, \pm 10$ . Basic cuts in Eq. (8) are also applied.



Cut	$\mathcal{A}^{\text{QCD}}$	$\mathcal{A}^{ZHjj, ZZjj}$	$\mathcal{A}^{\text{Signal}; \kappa=1}$
VBS cuts in Eq. (7)	0.086	0.630	0.631
$HH$ candidate cuts in Eqs. (10)-(13)	$1.3 \cdot 10^{-4}$	$3.1 \cdot 10^{-4}$	0.17
VBS cuts + $HH$ candidate cuts	$1.1 \cdot 10^{-5}$	$2.0 \cdot 10^{-4}$	0.081

Table 4: Predictions for acceptances of the VBS cuts given in Eq. (7), of the  $HH$  candidate cuts given in Eqs. (10)-(13), and of both sets of cuts combined for the multijet QCD background, for the combined  $pp \rightarrow HZjj \rightarrow b\bar{b}b\bar{b}jj$  and  $pp \rightarrow ZZjj \rightarrow b\bar{b}b\bar{b}jj$  background and for the signal with  $\kappa = 1$ . All the results are computed with the basic cuts in Eq. (8) already applied.

VBS cuts and the  $HH$  candidate cuts separately and together for the multijet QCD background, for the combined  $pp \rightarrow HZjj \rightarrow b\bar{b}b\bar{b}jj$  and  $pp \rightarrow ZZjj \rightarrow b\bar{b}b\bar{b}jj$  background and for the SM signal, for comparison.

Once we have the possible backgrounds under control, we can move on to fully explore the sensitivity to the Higgs self-coupling  $\lambda$  in  $pp \rightarrow b\bar{b}b\bar{b}jj$  events. In Fig. 12 we display the predictions for the total cross section of the total SM background (the sum of multijet QCD background and *quasi-irreducible* backgrounds) and of the signal for different values of  $\lambda$  as a function of the invariant mass of the four-bottom system  $M_{b\bar{b}b\bar{b}}$ . These distributions should be the analogous to those in Fig. 8 after the Higgs boson decays, as it is manifest since the signal curves follow the same tendency and are very similar except for the global factor of the Higgs-to-bottoms branching ratio. In this figure we can also see that the total SM background is of the same order of magnitude than the  $\kappa = 10$  and  $\kappa = -5$  signals, and it is even below the  $\kappa = -10$  signal prediction. This is a very interesting result, since it means that if, for example, the true value of  $\lambda$  was minus five times that of the SM, the LHC should be able to measure twice as many events as those expected from the SM background only in this VBS configuration. Similar conclusions can be extracted for other values of  $\kappa$ .

At the light of the encouraging previous results, our last step is to give quantitative predictions for the sensitivity to  $\lambda$  in  $pp \rightarrow b\bar{b}b\bar{b}jj$  processes at the LHC. To this end, we compute the statistical significance  $\mathcal{S}_{\text{stat}}$ , as defined in [60] by:

$$\mathcal{S}_{\text{stat}} = \sqrt{-2 \left( (N_S + N_B) \log \left( \frac{N_B}{N_S + N_B} \right) + N_S \right)}, \quad (14)$$

where  $N_S$  and  $N_B$  are the number of events of signal and background, respectively. Notice that for large  $N_S$ , this definition of  $\mathcal{S}_{\text{stat}}$  tends to the usual  $N_S / \sqrt{N_S + N_B}$  expression. This computation is going to be performed for four different values of the luminosity:  $L = 50, 300, 1000, 3000 \text{ fb}^{-1}$ , that correspond to a near-future LHC value for the current run ( $50 \text{ fb}^{-1}$ ), and to planned luminosities for the third run ( $300 \text{ fb}^{-1}$ ) and the High-Luminosity LHC (HL-LHC) ( $1000$  and  $3000 \text{ fb}^{-1}$ ) [61].

In Fig. 13 we present the results of the statistical significance of our signal,  $\mathcal{S}_{\text{stat}}$ , in  $pp \rightarrow b\bar{b}b\bar{b}jj$  events as a function of the value of  $\kappa$ , for the four luminosities considered. In the lower part of the left panel we also present the corresponding predictions for the total number of signal events,  $N_S$ , as a function of  $\kappa$ . The marked points correspond to our evaluated predictions. We show as well, in the right panel of this figure, our predictions for the value of the total integrated luminosity,  $L$ , as a function of the value of  $\kappa$  as well, that will be required to obtain a sensitivity to a given



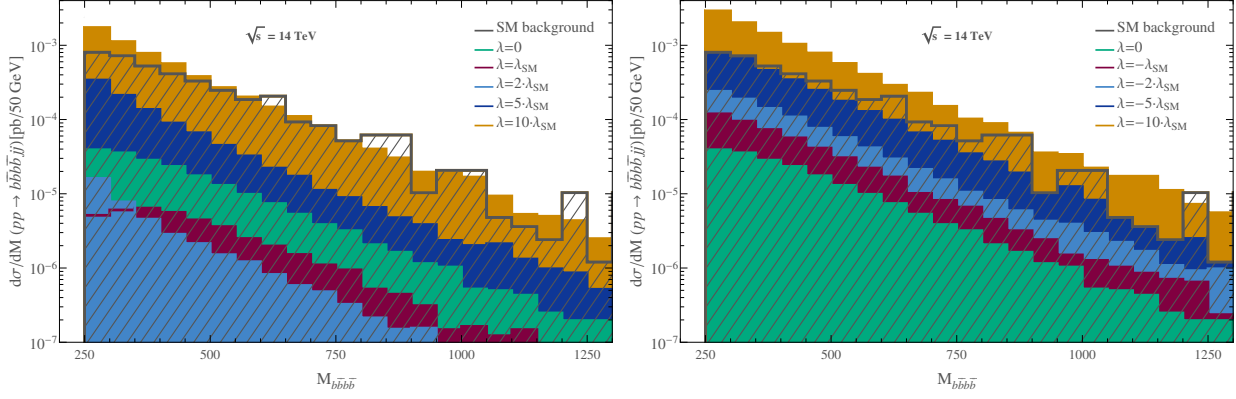


Figure 12: Predictions for the total cross section of the process  $pp \rightarrow b\bar{b}b\bar{b}jj$  as a function of the invariant mass of the four-bottom system  $M_{b\bar{b}b\bar{b}}$  for different values of the Higgs self-coupling  $\lambda$ . We display the predictions for the signal with positive (left panel) and negative (right panel) values of  $\lambda$  for comparison, as well as the irreducibles backgrounds and the multijet background. Cuts in Eq.(6) and VBS selection cuts presented in Eq.(7) have been applied. The center of mass energy has been set to  $\sqrt{s} = 14$  TeV.

$\kappa$  in  $pp \rightarrow b\bar{b}b\bar{b}jj$  events at the  $3\sigma$  and  $5\sigma$  level. In this plot, we have also marked the areas in luminosity where the number of predicted signal events  $N_S$  is below 1, 10 and 100, respectively, to get a reference of the statistics obtained.

From these plots, we can extract directly the conclusions on the sensitivity to  $\lambda$  in VBS processes at the LHC in  $pp \rightarrow b\bar{b}b\bar{b}jj$  events. The first thing one might observe is the high statistics and significances of the signal for most of the studied cases, except for the region close to the SM value, say for  $\kappa$  between 1 and 2. The second one is that, for the same absolute value of the coupling, the sensitivities to negative values of  $\kappa$  are higher than to positive values of  $\kappa$ . The third conclusion is that the LHC should be sensitive to very broad intervals of  $\kappa$ , even for the lowest luminosity considered,  $L = 50 \text{ fb}^{-1}$ , with high statistical significance. These means that VBS processes could allow to probe the value of  $\lambda$  with very good accuracy in the near future. More specifically, in Table 5 we show the summary of the predictions for the values of  $\kappa \equiv \lambda/\lambda_{SM}$  that the LHC would be able to probe in  $pp \rightarrow b\bar{b}b\bar{b}jj$  events, with a sensitivity equal or better than  $3\sigma$  ( $5\sigma$ ) for the four luminosities considered:  $L = 50, 300, 1000, 3000 \text{ fb}^{-1}$ .

These results are indeed very interesting, since the sensitivities to  $\lambda$  that one can obtain from

$L \text{ [fb}^{-1}\text{]}$	50	300	1000	3000
$\kappa > 0$	$\kappa > 5.4 \text{ (7.0)}$	$\kappa > 4.3 \text{ (4.8)}$	$\kappa > 3.7 \text{ (4.2)}$	$\kappa > 3.2 \text{ (3.7)}$
$\kappa < 0$	$\kappa < -2.4 \text{ (-3.8)}$	$\kappa < -1.0 \text{ (-1.7)}$	$\kappa < -0.3 \text{ (-0.8)}$	$\kappa < 0 \text{ (-0.2)}$

Table 5: Predictions for the values of  $\kappa \equiv \lambda/\lambda_{SM}$  that the LHC would be able to probe in  $pp \rightarrow b\bar{b}b\bar{b}jj$  events, with a sensitivity equal or better than  $3\sigma$  ( $5\sigma$ ) for the four luminosities considered:  $L = 50, 300, 1000, 3000 \text{ fb}^{-1}$ .

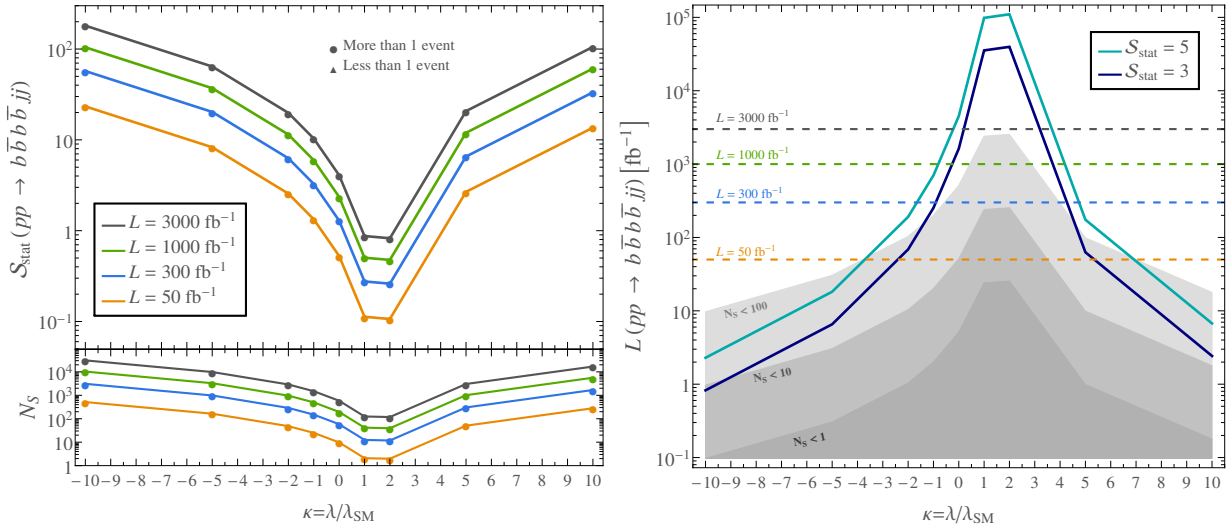


Figure 13: Prediction of the statistical significance,  $\mathcal{S}_{\text{stat}}$ , of the process  $pp \rightarrow b\bar{b}b\bar{b}jj$  for the four luminosities considered  $L = 50, 300, 1000, 3000 \text{ fb}^{-1}$  (left panel) and of the value of the luminosity that will be required to probe a given  $\kappa$  at the LHC at  $3\sigma$  and at  $5\sigma$  (right panel), as a function of the value of  $\kappa$ . The marked points represent our evaluations. The shadowed areas correspond to the regions where the number of predicted signal events  $N_S$  is below 1, 10 and 100. The center of mass energy has been set to  $\sqrt{s} = 14 \text{ TeV}$ .

studying VBS double Higgs production improve notably the present sensitivities. Even for the lowest luminosity considered,  $50 \text{ fb}^{-1}$ , the sensitivities are already better than those currently available in analyses that are focused on  $b\bar{b}b\bar{b}$  events coming from GGF production. On the other hand, it can be seen that the HL-LHC should be able to test very small deviations in the value of the Higgs self-coupling and that it should be sensitive to all the explored negative values for  $\kappa$ . Although the present work is a naive study, since it is performed at the parton level and does not take into account hadronization and detector response simulation, the results in Table 5 show that the VBS production channel could be very promising to measure the true value of  $\lambda$ , and, therefore, to understand the nature of the Higgs mechanism.

### 3.3 Analysis after Higgs boson decays: sensitivity to $\lambda$ in $pp \rightarrow b\bar{b}\gamma\gamma jj$ events

The  $pp \rightarrow b\bar{b}b\bar{b}jj$  process is, as we have seen, a very promising channel to study the Higgs self-coupling at the LHC due to its large event rates. However, it is clear that it suffers from quite severe backgrounds, coming specially from multijet QCD events, so one could think of studying complementary channels with smaller rates but with a cleaner experimental signature. This is the reason why we would like to explore the case in which one of the Higgs bosons decays to a  $b$ -quark pair, as before, while the other one decays to two photons through gauge bosons and fermion loops. This implies a large reduction factor in statistics due to the comparative low branching ratio  $\text{BR}(H \rightarrow \gamma\gamma) \sim 0.2\%$ , a factor 0.003 smaller than that of  $H \rightarrow b\bar{b}$ .

The analysis of the process  $pp \rightarrow HHjj \rightarrow b\bar{b}\gamma\gamma jj$  implies to go through its main backgrounds as well. We will consider in this section the same *quasi-irreducible* background  $ZH$  of the previous case, since the  $ZH$  final state can also lead to processes with two photons and two bottoms,  $pp \rightarrow HZjj \rightarrow b\bar{b}\gamma\gamma jj$ , coming from the decays of the  $H$  and the  $Z$ . We also consider the mixed

QCD-EW reducible background, of  $\mathcal{O}(\alpha \cdot \alpha_S^2)$  at the amplitude level, that should be the most severe one.

As we did before, to study signal and background, we first need to establish a set of cuts that ensure particle detection, so we apply the following basic cuts:

$$p_{T_{j,b}} > 20 \text{ GeV}; \quad p_{T_\gamma} > 18 \text{ GeV}; \quad |\eta_j| < 5; \quad |\eta_{b,\gamma}| < 2.5; \quad \Delta R_{jj,jb,\gamma\gamma,\gamma b,\gamma j} > 0.4; \quad \Delta R_{bb} > 0.2, \quad (15)$$

and afterwards, to reject the QCD-EW and the *quasi-irreducible* backgrounds we will apply first the VBS cuts given in Eq. (7) and subsequently the following kinematical cuts given by CMS in [33]:

$$p_{T_{\gamma l}}/M_{\gamma\gamma} > 1/3; \quad p_{T_{\gamma s}}/M_{\gamma\gamma} > 1/4, \quad (16)$$

where  $l$  and  $s$  stand for leading (highest  $p_T$  value) and subleading photons, and where  $M_{\gamma\gamma}$  is the invariant mass of the photon pair. The final ingredient is to apply the  $\chi_{HH}$  cut, taking now into account that we have a  $b$ -quark pair and a photon pair in the final state:

$$\chi_{HH} = \sqrt{\left(\frac{M_{bb} - m_H}{0.05 m_H}\right)^2 + \left(\frac{M_{\gamma\gamma} - m_H}{0.05 m_H}\right)^2} < 1. \quad (17)$$

This ensures that the two  $b$ -quarks and the two photons come from the decay of a Higgs particle.

With this set of cuts, we present in Fig. 14 the predictions for the total cross section of the process  $pp \rightarrow b\bar{b}\gamma\gamma jj$  as a function of the invariant mass of the  $b\bar{b}\gamma\gamma$  system  $M_{b\bar{b}\gamma\gamma}$ , for different values of the Higgs self-coupling  $\lambda$ . We also display the prediction for the total SM background (sum of the QCD-EW and the quasi-irreducible background) for comparison. Once again, one can see that the signal distributions for different values of  $\kappa$  are very similar to those shown in Fig. 8, and that the main difference is due to the reduction factor of the branching ratios into photons and into  $b$ -quarks. They are very similar, too, to the results of the  $b\bar{b}bbjj$  final state, in Fig. 12, although two-three orders of magnitude smaller. The background is, however, very different with respect to the one for  $b\bar{b}bbjj$  events. It is smaller in comparison with the signal, specially at high  $M_{b\bar{b}\gamma\gamma}$ , since it decreases much more steeply. Therefore, we would expect to have good sensitivities to the Higgs self-coupling despite the lower rates of the process involving photons. For completeness, we display in Table 6 the predictions for the total cross section of the signal, for the set of  $\kappa$  values considered, and after applying all cuts given in Eq. (7) and in Eqs. (15)-(17). The prediction for the cross section of the total SM background for this same cuts amounts to  $\sigma_{\text{Background}} = 1.4 \cdot 10^{-6}$  pb.

In Fig. 15 we show the predictions for the statistical significance  $\mathcal{S}_{\text{stat}}$ , computed in the same way as in the previous section, making use of Eq. (14), for the four luminosities considered previously,  $L = 50, 300, 1000, 3000 \text{ fb}^{-1}$ . We also show the predictions of the final number of signal events,  $N_S$  as a function of  $\kappa$ , for these same luminosities. On the right panel of this figure we present

$\kappa$	0	1	-1	2	-2	5	-5	10	-10
$\sigma_{\text{Signal}} \cdot 10^6 \text{ [pb]}$	2.0	0.7	4.5	0.5	8.0	6.4	25.2	38.4	76.0

Table 6: Predictions for the total cross section of the signal  $pp \rightarrow b\bar{b}\gamma\gamma jj$  after imposing all the selection criteria, VBS cuts given in Eq. (7) and cuts given in Eqs. (16) and (17) for all the values of  $\kappa$  considered in this work:  $\kappa = 0, \pm 1, \pm 2, \pm 5, \pm 10$ . The cross section of the SM background for this same cuts amounts to  $\sigma_{\text{Background}} = 1.4 \cdot 10^{-6}$  pb. Basic cuts in Eq. (15) are also applied.

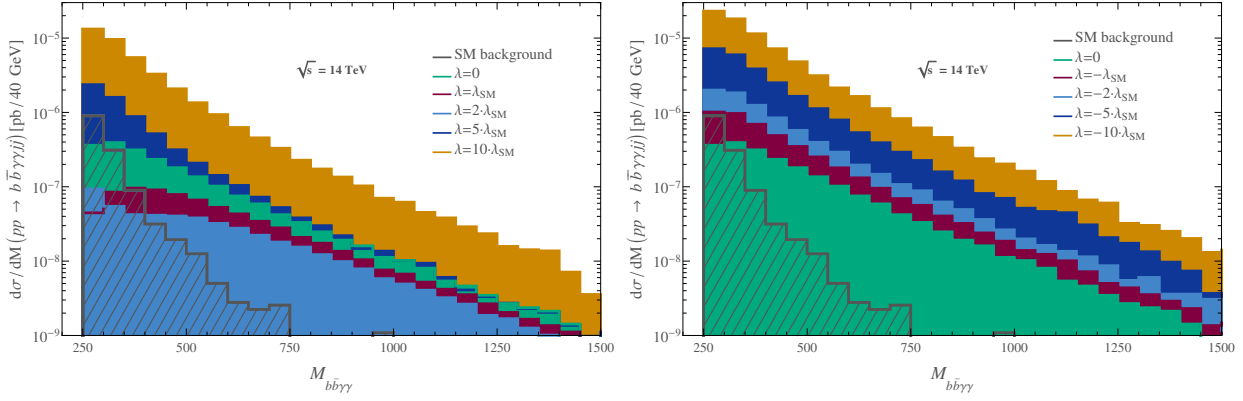


Figure 14: Predictions for the total cross section of the process  $pp \rightarrow b\bar{b}\gamma\gamma jj$  as a function of the invariant mass of the  $b\bar{b}\gamma\gamma$  system  $M_{b\bar{b}\gamma\gamma}$  for different values of the Higgs self-coupling  $\lambda$ . We display the predictions for the signal with positive (left panel) and negative (right panel) values of  $\lambda$  for comparison, as well as the total SM background. Cuts in Eqs.(15)-(17) and VBS selection cuts presented in Eq.(7) have been applied. The center of mass energy is set to  $\sqrt{s} = 14$  TeV.

the prediction for the value of the luminosity that will be required to probe a given  $\kappa$  value with sensitivities at  $3\sigma$  and  $5\sigma$ , as a function of the value of  $\kappa$ . In these plots, due to the lower statistics of this process, some of the computed significances correspond to scenarios in which there is not even one signal event. The concrete predictions for these signal event rates can be read from the lower plot of the left panel.

At the light of these figures, we can again extract the conclusions on the sensitivity to the Higgs self-coupling at the LHC in VBS processes, this time in  $pp \rightarrow b\bar{b}\gamma\gamma jj$  events. One might notice that, although the results are less encouraging than those of  $pp \rightarrow b\bar{b}b\bar{b}jj$  events, this channel could also be very useful to measure the value of  $\lambda$ . Analogously to the previous section, in Table 7 we present the values of  $\kappa \equiv \lambda/\lambda_{SM}$  that would be accesible at the LHC in these type of events,  $pp \rightarrow b\bar{b}\gamma\gamma jj$ , with a statistical significance equal or better than  $3\sigma(5\sigma)$ , for the four luminosities considered.

These results show again that the values of  $\kappa$  than can be probed in the future at LHC through the study of VBS processes leading to the final state  $b\bar{b}\gamma\gamma jj$  could be competitive with those of GGF. Except for the lowest luminosity considered,  $L = 50 \text{ fb}^{-1}$ , where the signal rates found at the parton level are too low as to survive the extra factors suppression due to the missing detector

$L \text{ [fb}^{-1}]$	50	300	1000	3000
$\kappa > 0$	$\kappa > 9.9 \text{ (14.2)}$	$\kappa > 6.4 \text{ (8.4)}$	$\kappa > 4.6 \text{ (6.0)}$	$\kappa > 3.8 \text{ (4.7)}$
$\kappa < 0$	$\kappa < -6.7 \text{ (-10.0)}$	$\kappa < -2.7 \text{ (-4.6)}$	$\kappa < -1.1 \text{ (-2.3)}$	$\kappa < -0.2 \text{ (-1.0)}$

Table 7: Predictions for the values of  $\kappa \equiv \lambda/\lambda_{SM}$  that the LHC would be able to probe in  $pp \rightarrow b\bar{b}\gamma\gamma jj$  events, with a sensitivity equal or better than  $3\sigma$  ( $5\sigma$ ) for the four luminosities considered:  $L = 50, 300, 1000, 3000 \text{ fb}^{-1}$ .

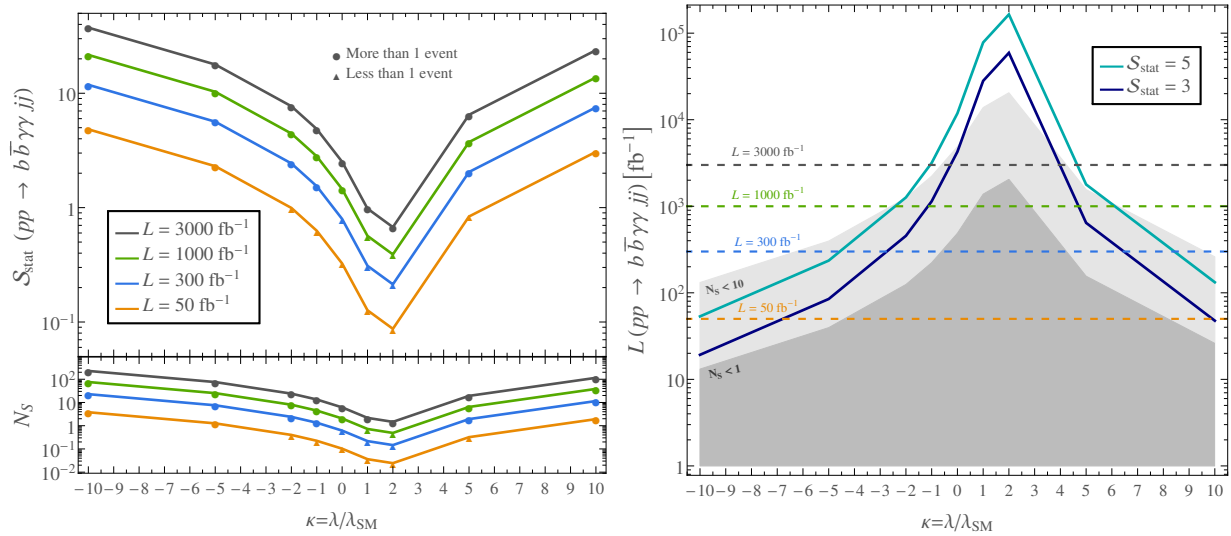


Figure 15: Prediction of the statistical significance,  $\mathcal{S}_{\text{stat}}$ , of the process  $pp \rightarrow b\bar{b}\gamma\gamma jj$  for the four luminosities considered  $L = 50, 300, 1000, 3000 \text{ fb}^{-1}$  (left panel) and of the value of the luminosity that will be required to probe a given  $\kappa$  at the LHC at  $3\sigma$  and at  $5\sigma$  (right panel), as a function of the value of  $\kappa$ . The marked points represent our evaluations. The shadowed areas correspond to the regions where the number of predicted signal events  $N_S$  is below 1, and 10. The center of mass energy has been set to  $\sqrt{s} = 14 \text{ TeV}$ .

efficiencies, hadronization effects etc, the sensitivities found are a little better than those obtained at present by studying searches of  $b\bar{b}\gamma\gamma$  final states coming from GGF. Also, the HL-LHC should be able to probe deviations in  $\lambda$  very efficiently in this channel.

We would like to point out once again that the present study is very naive in the sense that all simulations are made at the parton level and therefore, a more complete study, including hadronization effects and detection efficiencies, might change a little bit the results. Nevertheless, the fact that we obtain interesting and competitive predictions for the sensitivities to probe deviations in the Higgs self-coupling respect to the SM value makes us believe that VBS double Higgs production is a very promising channel to explore the BSM Higgs sector self-interactions.

## 4 Conclusions

Being able to determine with precision the value of the Higgs self-coupling  $\lambda$  would allow us to understand the true nature of the Higgs mechanism and, therefore, of the scalar sector of the SM. In particular, an independent measurement of  $\lambda$  and  $m_H$  will be crucial in this understanding. At the LHC, the most sensitive channel to this coupling  $\lambda$  is that of double Higgs production, that can take place through several initial configurations. Most of the theoretical and experimental studies of  $HH$  production focus on gluon-gluon fusion since it benefits from the largest rates. Nevertheless, double Higgs production by vector boson scattering has important advantages with respect to gluon-gluon fusion that, despite its lower statistics, make of it a very promising and competitive channel to probe the Higgs self coupling at the LHC. These features have motivated our study here.

In the present work, we have analyzed the sensitivity to  $\lambda$  in double Higgs production via vector

boson scattering at the LHC, taking advantage of the fact that these processes have very characteristic kinematics that allow to select them very efficiently against competing SM backgrounds. We have first explored and characterized the VBS subprocesses of our interest,  $WW \rightarrow HH$  and  $ZZ \rightarrow HH$ , both for the SM with  $\lambda = \lambda_{SM}$ , and for BSM scenarios with  $\lambda = \kappa \lambda_{SM}$ , considering values of  $\kappa$  between 10 and -10, to move afterwards to the LHC scenario. We have then studied the process  $pp \rightarrow HHjj$ , in order to understand the properties of this scattering, and finally we have explored and provided quantitative results for the sensitivity to the Higgs self-coupling after the Higgs decays.

We have focused mainly on the  $pp \rightarrow b\bar{b}b\bar{b}jj$  process since it benefits from the largest rates. After applying all our selection criteria, based on the VBS characteristic kinematical configuration and in the  $HH$  candidates reconstruction, we give predictions for the sensitivity to  $\lambda$  in  $pp \rightarrow b\bar{b}b\bar{b}jj$  events at the parton level for  $\sqrt{s} = 14$  TeV and for different future expected luminosities:  $L = 50, 300, 1000, 3000 \text{ fb}^{-1}$ . Our main results for this channel are summarized in Table 5 and in Fig. 13, in which we present the values of  $\kappa$  that the LHC would be sensitive to at the  $3\sigma$  and at the  $5\sigma$  level. The sensitivities we obtain are, even for the lowest luminosity, better than those currently available for  $HH$  production via GGF. Furthermore, our predictions show that the HL-LHC should be able to probe small deviations in  $\lambda$  respect to the SM value, reaching very good sensitivities with the highest luminosity to up to  $\kappa \sim 3$  at the  $3\sigma$  level in the best scenario for positive values. In the case of negative values, the HL-LHC would be sensitive to all the  $\kappa < 0$  values that have been considered in this work.

We give as well predictions for  $pp \rightarrow b\bar{b}\gamma\gamma jj$  events, also at the parton level and for  $\sqrt{s} = 14$  TeV, due to the fact that it provides a cleaner, although with smaller rates, signature. The results of the sensitivities to the Higgs self-coupling in this channel, after applying the proper selection criteria, are collected in Table 7 and in Fig. 15. Again, we obtain better results than those already available for  $b\bar{b}\gamma\gamma$  events coming from gluon-gluon fusion, except for the lowest luminosity considered, where the signal rates found are too low. Interestingly, we show that for bigger luminosities, very small deviations in  $\lambda$  could also be measured in this channel.

The present study shows that double Higgs production via vector boson scattering is a viable and promising window to measure the Higgs self-coupling and to deeply understand the scalar sector of the SM. Although all simulations are performed at the parton level, without hadronization or detector response simulation, and should be understood as a naive first approximation, we obtain very competitive results for the sensitivity to  $\lambda$  at the LHC. Because of this, we believe that the vector boson scattering  $HH$  production channel will lead to very interesting (and complementary to those of gluon-gluon fusion) findings about the true nature of the Higgs boson.

## Acknowledgments

The authors would like to warmly thank Michelangelo L. Mangano for his invaluable help and generosity in guiding us with the use of AlpGen, taking active part in the running of this MonteCarlo, which has been a very important part of the QCD background evaluation for this work. We would also like to thank Juan Antonio Aguilar Saavedra for fruitful discussions and Richard Ruiz for his help and suggestions in the use of MadGraph. C.G.G. wishes to thank Xabier Marcano, Víctor Martín Lozano and Javier Quilis for supportive and helpful conversations. E.A. warmly thanks IFT of Madrid for its hospitality hosting him during the completion of this work. This work is supported by the European Union through the ITN ELUSIVES H2020-MSCA-ITN-2015//674896 and the RISE INVISIBLESPLUS H2020-MSCA-RISE-2015//690575, by the CICYT through the projects FPA2016-78645-P, by the Spanish Consolider-Ingenio 2010 Programme CPAN (CSD2007-00042) and by the Spanish MINECO's "Centro de Excelencia Severo Ochoa" Programme under



grant SEV-2012-0249. This work This work has been supported by CONICET (E.A.).

## References

- [1] ATLAS collaboration, G. Aad et al., *Observation of a new particle in the search for the Standard Model Higgs boson with the ATLAS detector at the LHC*, *Phys. Lett. B* **716** (2012) 1 [1207.7214].
- [2] CMS collaboration, S. Chatrchyan et al., *Observation of a new boson at a mass of 125 GeV with the CMS experiment at the LHC*, *Phys. Lett. B* **716** (2012) 30 [1207.7235].
- [3] P. W. Higgs, *Broken symmetries, massless particles and gauge fields*, *Phys. Lett.* **12** (1964) 132.
- [4] F. Englert and R. Brout, *Broken Symmetry and the Mass of Gauge Vector Mesons*, *Phys. Rev. Lett.* **13** (1964) 321.
- [5] P. W. Higgs, *Broken Symmetries and the Masses of Gauge Bosons*, *Phys. Rev. Lett.* **13** (1964) 508.
- [6] P. W. Higgs, *Spontaneous Symmetry Breakdown without Massless Bosons*, *Phys. Rev.* **145** (1966) 1156.
- [7] F. Simon, *Prospects for Precision Higgs Physics at Linear Colliders*, *PoS ICHEP2012* (2013) 066 [1211.7242].
- [8] S. Dawson et al., *Working Group Report: Higgs Boson*, in *Proceedings, 2013 Community Summer Study on the Future of U.S. Particle Physics: Snowmass on the Mississippi (CSS2013): Minneapolis, MN, USA, July 29-August 6, 2013*, 2013, **1310.8361**, <http://inspirehep.net/record/1262795/files/arXiv:1310.8361.pdf>.
- [9] H. Baer, T. Barklow, K. Fujii, Y. Gao, A. Hoang, S. Kanemura et al., *The International Linear Collider Technical Design Report - Volume 2: Physics*, **1306.6352**.
- [10] H. Abramowicz et al., *Higgs physics at the CLIC electron-positron linear collider*, *Eur. Phys. J. C* **77** (2017) 475 [1608.07538].
- [11] LHC HIGGS CROSS SECTION WORKING GROUP collaboration, D. de Florian et al., *Handbook of LHC Higgs Cross Sections: 4. Deciphering the Nature of the Higgs Sector*, **1610.07922**.
- [12] U. Baur, T. Plehn and D. L. Rainwater, *Probing the Higgs selfcoupling at hadron colliders using rare decays*, *Phys. Rev. D* **69** (2004) 053004 [hep-ph/0310056].
- [13] R. Grober and M. Muhlleitner, *Composite Higgs Boson Pair Production at the LHC*, *JHEP* **06** (2011) 020 [1012.1562].
- [14] M. J. Dolan, C. Englert and M. Spannowsky, *Higgs self-coupling measurements at the LHC*, *JHEP* **10** (2012) 112 [1206.5001].
- [15] A. Papaefstathiou, L. L. Yang and J. Zurita, *Higgs boson pair production at the LHC in the  $b\bar{b}W^+W^-$  channel*, *Phys. Rev. D* **87** (2013) 011301 [1209.1489].
- [16] J. Baglio, A. Djouadi, R. Gröber, M. M. Mühlleitner, J. Quevillon and M. Spira, *The measurement of the Higgs self-coupling at the LHC: theoretical status*, *JHEP* **04** (2013) 151 [1212.5581].
- [17] D. de Florian and J. Mazzitelli, *Higgs Boson Pair Production at Next-to-Next-to-Leading Order in QCD*, *Phys. Rev. Lett.* **111** (2013) 201801 [1309.6594].
- [18] R. Frederix, S. Frixione, V. Hirschi, F. Maltoni, O. Mattelaer, P. Torrielli et al., *Higgs pair production at the LHC with NLO and parton-shower effects*, *Phys. Lett. B* **732** (2014) 142 [1401.7340].



- [19] L.-S. Ling, R.-Y. Zhang, W.-G. Ma, L. Guo, W.-H. Li and X.-Z. Li, *NNLO QCD corrections to Higgs pair production via vector boson fusion at hadron colliders*, *Phys. Rev.* **D89** (2014) 073001 [[1401.7754](#)].
- [20] F. Goertz, A. Papaefstathiou, L. L. Yang and J. Zurita, *Higgs boson pair production in the  $D=6$  extension of the SM*, *JHEP* **04** (2015) 167 [[1410.3471](#)].
- [21] A. Azatov, R. Contino, G. Panico and M. Son, *Effective field theory analysis of double Higgs boson production via gluon fusion*, *Phys. Rev.* **D92** (2015) 035001 [[1502.00539](#)].
- [22] D. A. Dicus, C. Kao and W. W. Repko, *Interference effects and the use of Higgs boson pair production to study the Higgs trilinear self coupling*, *Phys. Rev.* **D92** (2015) 093003 [[1504.02334](#)].
- [23] S. Dawson, A. Ismail and I. Low, *What's in the loop? The anatomy of double Higgs production*, *Phys. Rev.* **D91** (2015) 115008 [[1504.05596](#)].
- [24] H.-J. He, J. Ren and W. Yao, *Probing new physics of cubic Higgs boson interaction via Higgs pair production at hadron colliders*, *Phys. Rev.* **D93** (2016) 015003 [[1506.03302](#)].
- [25] J. K. Behr, D. Bortoletto, J. A. Frost, N. P. Hartland, C. Issever and J. Rojo, *Boosting Higgs pair production in the  $b\bar{b}b\bar{b}$  final state with multivariate techniques*, *Eur. Phys. J.* **C76** (2016) 386 [[1512.08928](#)].
- [26] F. Bishara, R. Contino and J. Rojo, *Higgs pair production in vector-boson fusion at the LHC and beyond*, *Eur. Phys. J.* **C77** (2017) 481 [[1611.03860](#)].
- [27] S. Banerjee, C. Englert, M. L. Mangano, M. Selvaggi and M. Spannowsky,  *$hh + jet$  production at 100 TeV*, *Eur. Phys. J.* **C78** (2018) 322 [[1802.01607](#)].
- [28] D. Gonçalves, T. Han, F. Kling, T. Plehn and M. Takeuchi, *Higgs boson pair production at future hadron colliders: From kinematics to dynamics*, *Phys. Rev.* **D97** (2018) 113004 [[1802.04319](#)].
- [29] ATLAS collaboration, M. Aaboud et al., *Search for pair production of Higgs bosons in the  $b\bar{b}b\bar{b}$  final state using proton-proton collisions at  $\sqrt{s} = 13$  TeV with the ATLAS detector*, *Phys. Rev.* **D94** (2016) 052002 [[1606.04782](#)].
- [30] CMS collaboration, C. Collaboration, *Search for non-resonant pair production of Higgs bosons in the  $b\bar{b}b\bar{b}$  final state with 13 TeV CMS data*, CMS-PAS-HIG-16-026 (2016) .
- [31] CMS collaboration, C. Collaboration, *Search for Higgs boson pair production in the final state containing two photons and two bottom quarks in proton-proton collisions at  $\sqrt{s} = 13$  TeV*, CMS-PAS-HIG-17-008 (2017) .
- [32] ATLAS collaboration, M. Aaboud et al., *Search for pair production of Higgs bosons in the  $b\bar{b}b\bar{b}$  final state using proton-proton collisions at  $\sqrt{s} = 13$  TeV with the ATLAS detector*, [1804.06174](#).
- [33] CMS collaboration, A. M. Sirunyan et al., *Search for Higgs boson pair production in the  $\gamma\gamma b\bar{b}$  final state in  $pp$  collisions at  $\sqrt{s} = 13$  TeV*, [1806.00408](#).
- [34] ATLAS collaboration, M. Aaboud et al., *Search for resonant  $WZ$  production in the fully leptonic final state in proton-proton collisions at  $\sqrt{s} = 13$  TeV with the ATLAS detector*, [1806.01532](#).
- [35] ATLAS collaboration, M. Aaboud et al., *Search for Higgs boson pair production in the  $\gamma\gamma b\bar{b}$  final state with 13 TeV  $pp$  collision data collected by the ATLAS experiment*, [1807.04873](#).
- [36] K. Doroba, J. Kalinowski, J. Kuczmarski, S. Pokorski, J. Rosiek, M. Szleper et al., *The  $W_L W_L$  Scattering at the LHC: Improving the Selection Criteria*, *Phys. Rev.* **D86** (2012) 036011 [[1201.2768](#)].
- [37] M. Szleper, *The Higgs boson and the physics of  $WW$  scattering before and after Higgs discovery*, [1412.8367](#).

- [38] M. Fabbrichesi, M. Pinamonti, A. Tonero and A. Urbano, *Vector boson scattering at the LHC: A study of the  $WW \rightarrow WW$  channels with the Warsaw cut*, *Phys. Rev.* **D93** (2016) 015004 [[1509.06378](#)].
- [39] R. L. Delgado, A. Dobado, D. Espriu, C. Garcia-Garcia, M. J. Herrero, X. Marcano et al., *Production of vector resonances at the LHC via WZ-scattering: a unitarized EChL analysis*, *JHEP* **11** (2017) 098 [[1707.04580](#)].
- [40] PARTICLE DATA GROUP collaboration, M. Tanabashi et al., *Review of Particle Physics*, *Phys. Rev.* **D98** (2018) 030001.
- [41] ATLAS collaboration, G. Aad et al., *Evidence for Electroweak Production of  $W^\pm W^\pm jj$  in  $pp$  Collisions at  $\sqrt{s} = 8$  TeV with the ATLAS Detector*, *Phys. Rev. Lett.* **113** (2014) 141803 [[1405.6241](#)].
- [42] ATLAS collaboration, G. Aad et al., *Measurements of  $W^\pm Z$  production cross sections in  $pp$  collisions at  $\sqrt{s} = 8$  TeV with the ATLAS detector and limits on anomalous gauge boson self-couplings*, *Phys. Rev.* **D93** (2016) 092004 [[1603.02151](#)].
- [43] ATLAS collaboration, M. Aaboud et al., *Search for anomalous electroweak production of  $WW/WZ$  in association with a high-mass dijet system in  $pp$  collisions at  $\sqrt{s} = 8$  TeV with the ATLAS detector*, *Phys. Rev.* **D95** (2017) 032001 [[1609.05122](#)].
- [44] ATLAS collaboration, M. Aaboud et al., *Measurement of  $W^\pm W^\pm$  vector-boson scattering and limits on anomalous quartic gauge couplings with the ATLAS detector*, *Phys. Rev.* **D96** (2017) 012007 [[1611.02428](#)].
- [45] ATLAS collaboration, M. Aaboud et al., *Studies of  $Z\gamma$  production in association with a high-mass dijet system in  $pp$  collisions at  $\sqrt{s} = 8$  TeV with the ATLAS detector*, *JHEP* **07** (2017) 107 [[1705.01966](#)].
- [46] ATLAS collaboration, T. A. collaboration, *Observation of electroweak production of a same-sign  $W$  boson pair in association with two jets in  $pp$  collisions at  $\sqrt{s} = 13$  TeV with the ATLAS detector*, *ATLAS-CONF-2018-030* (2018) .
- [47] ATLAS collaboration, T. A. collaboration, *Observation of electroweak  $W^\pm Z$  boson pair production in association with two jets in  $pp$  collisions at  $\sqrt{s} = 13$  TeV with the ATLAS Detector*, *ATLAS-CONF-2018-033* (2018) .
- [48] CMS collaboration, V. Khachatryan et al., *Study of vector boson scattering and search for new physics in events with two same-sign leptons and two jets*, *Phys. Rev. Lett.* **114** (2015) 051801 [[1410.6315](#)].
- [49] CMS collaboration, V. Khachatryan et al., *Measurement of electroweak-induced production of  $W\gamma$  with two jets in  $pp$  collisions at  $\sqrt{s} = 8$  TeV and constraints on anomalous quartic gauge couplings*, *JHEP* **06** (2017) 106 [[1612.09256](#)].
- [50] CMS collaboration, V. Khachatryan et al., *Measurement of the cross section for electroweak production of  $Z\gamma$  in association with two jets and constraints on anomalous quartic gauge couplings in proton-proton collisions at  $\sqrt{s} = 8$  TeV*, *Phys. Lett.* **B770** (2017) 380 [[1702.03025](#)].
- [51] CMS collaboration, A. M. Sirunyan et al., *Measurement of vector boson scattering and constraints on anomalous quartic couplings from events with four leptons and two jets in proton-proton collisions at  $\sqrt{s} = 13$  TeV*, *Phys. Lett.* **B774** (2017) 682 [[1708.02812](#)].
- [52] CMS collaboration, A. M. Sirunyan et al., *Observation of electroweak production of same-sign  $W$  boson pairs in the two jet and two same-sign lepton final state in proton-proton collisions at  $\sqrt{s} = 13$  TeV*, *Phys. Rev. Lett.* **120** (2018) 081801 [[1709.05822](#)].
- [53] CMS collaboration, A. M. Sirunyan et al., *Electroweak production of two jets in association with a  $Z$  boson in proton-proton collisions at  $\sqrt{s} = 13$  TeV*, *Submitted to: Eur. Phys. J. C* (2017) [[1712.09814](#)].

- [54] CMS collaboration, C. Collaboration, *Measurements of the  $pp \rightarrow WZ$  inclusive and differential production cross section and constraints on charged anomalous triple gauge couplings at  $\sqrt{s} = 13$  TeV., CMS-PAS-SMP-18-002* (2018) .
- [55] CMS collaboration, C. Collaboration, *Measurement of electroweak  $WZ$  production and search for new physics in  $pp$  collisions at  $\sqrt{s} = 13$  TeV, CMS-PAS-SMP-18-001* (2018) .
- [56] J. Alwall, R. Frederix, S. Frixione, V. Hirschi, F. Maltoni, O. Mattelaer et al., *The automated computation of tree-level and next-to-leading order differential cross sections, and their matching to parton shower simulations*, *JHEP* **07** (2014) 079 [[1405.0301](#)].
- [57] NNPDF collaboration, R. D. Ball, V. Bertone, S. Carrazza, L. Del Debbio, S. Forte, A. Guffanti et al., *Parton distributions with QED corrections*, *Nucl. Phys.* **B877** (2013) 290 [[1308.0598](#)].
- [58] M. L. Mangano, M. Moretti, F. Piccinini, R. Pittau and A. D. Polosa, *ALPGEN, a generator for hard multiparton processes in hadronic collisions*, *JHEP* **07** (2003) 001 [[hep-ph/0206293](#)].
- [59] CTEQ collaboration, H. L. Lai, J. Huston, S. Kuhlmann, J. Morfin, F. I. Olness, J. F. Owens et al., *Global QCD analysis of parton structure of the nucleon: CTEQ5 parton distributions*, *Eur. Phys. J.* **C12** (2000) 375 [[hep-ph/9903282](#)].
- [60] G. Cowan, K. Cranmer, E. Gross and O. Vitells, *Asymptotic formulae for likelihood-based tests of new physics*, *Eur. Phys. J.* **C71** (2011) 1554 [[1007.1727](#)].
- [61] A. Barachetti, L. Rossi and A. Szeberenyi, *Final Project Report: Deliverable D1.14, CERN-ACC-2016-0007* (2016) .